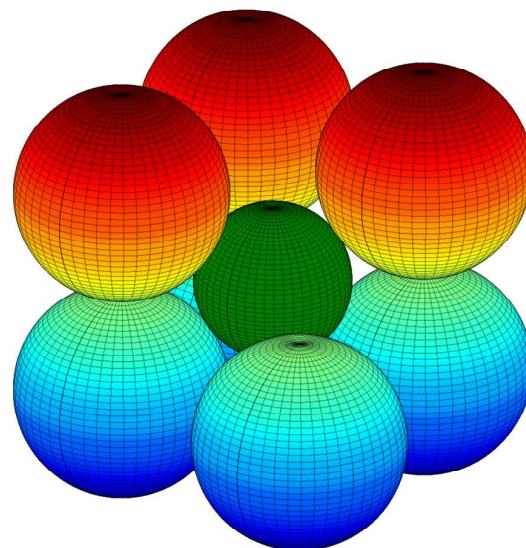


# CHALMERS



## Modulation for Point to Point Microwave Radio Links

*Master of Science thesis at Department of Signals and Systems-  
Chalmers University of Technology, Göteborg in collaboration with  
Ericsson AB, Mölndal, Sweden*

Anser Ahmed and Keerthi Kumar Nagalapur

# Modulation for Point to Point Microwave Radio Links

*Master of Science thesis at Department of Signals and Systems-  
Chalmers University of Technology, Göteborg in collaboration with  
Ericsson AB, Mölndal, Sweden*

Anser Ahmed and Keerthi Kumar Nagalapur

Examiner: **Professor Erik Agrell**

Chalmers, Signals and Systems

Supervisors: **Dr. Lei Bao**

Ericsson AB, Ericsson Research

**Dr. Mats Rydström**

Ericsson AB

**Mr. Lofollah Beygi**

Doctoral Student, Chalmers, Signals and Systems

Master's Thesis EX009/2012

Göteborg, Sweden. August 2011 - March 2012

*This page has been intentionally left blank.*

## Abstract

*The drastic increase of traffic in cellular networks due to the introduction of mobile broadband technologies such as HSPA and LTE has created a need to improve the data throughput in the back-hauling networks and thus over the microwave links. The scarcity and the high cost of spectrum have influenced telecommunication fraternity to come up with spectrally efficient communication systems. The techniques like line-of-sight MIMO and Dual Polarization-multiplexing have enabled the increase in spectral efficiency. Though the above techniques have improved the spectral efficiency significantly, further improvements have to be considered.*

*Dual polarization-multiplexing and spatially-separated line-of-sight MIMO techniques have given rise to parallel streams for communication. The existing systems modulate and demodulate these parallel streams independently. In this thesis, the idea of using the parallel streams together for modulation and detection (joint modulation and detection) is considered. This allows the signal space to move from two to higher dimensions. In this thesis the modulation formats in four-dimensional (4-D) space are examined. Further, the same idea has been extended to eight dimensions.*

*The performance of modulation formats in four and eight dimensions are compared with the standard QAM constellations. The introduced modulation formats are shown to be power and spectrally efficient. The performance of the modulation formats is studied for AWGN and partially coherent AWGN channel models and capacity curves are plotted. Finally, we have discussed low complexity detectors for the joint modulations which make the modulation formats practically feasible.*

# Acknowledgement

This report is the result of our master's thesis work carried out at Ericsson research, Mölndal. The thesis also fulfils the partial requirement for the Master's Degree "Communication Engineering" at Chalmers University of Technology, Göteborg, Sweden.

We would like to thank Lei Bao, Lotfollah Beygi and Mats Rydström for being our supervisors. Their timely and good advice made the completion of this thesis possible. We would also like to thank Professor Erik Agrell for being our examiner and Thomas Lewin, Manager at Ericsson Research, Mölndal. Finally we would like to show our gratitude to all the members at TLU, Ericsson Research, Mölndal for providing us a lively and motivating environment.

# Contents

Notation	viii
<b>1 Introduction</b>	<b>1</b>
1.1 Background	1
1.1.1 Four-dimensional modulation	1
1.2 Problem Description	2
1.3 Thesis Organization	3
<b>2 Wireless Microwave Systems</b>	<b>4</b>
2.1 Shannon Communication System Model	4
2.2 Channel Model	5
2.2.1 AWGN channel	5
2.2.2 PC-AWGN channel	6
2.2.3 Fading	6
2.2.4 Intersymbol Interference	7
2.3 Microwave Systems	7
2.3.1 Dual Polarized Systems	7
2.3.2 LoS MIMO for Microwave Systems	8
2.3.3 Cross Polarization Interference Cancellation	10
2.3.4 $4 \times 4$ SS DP LoS MIMO	11
<b>3 Performance of Modulation Formats</b>	<b>13</b>
3.1 Modulation Formats	13
3.2 Definitions	15
3.2.1 Average Symbol Energy ( $E_s$ )	15
3.2.2 Symbol Error and Bit Error Rates	15
3.2.3 Receiver Sensitivity	16
3.2.4 Spectral Efficiency	16
3.2.5 Asymptotic Power Efficiency	17
3.3 Circle Approximation of a Symbol	17
3.4 Power Efficient Modulation Formats in Two and Three Dimensions	21
3.4.1 Kissing Number	22
3.5 Comparison of Modulation Formats	23

<b>4</b>	<b>Four-Dimensional Modulation Formats</b>	<b>25</b>
4.1	Dual Polarization Multiplexing . . . . .	25
4.1.1	Four-Dimensional view of Dual Polarized Systems . . . . .	26
4.2	Geometry of the Cubic Constellations . . . . .	27
4.2.1	A Spectrally Efficient Modulation in Four Dimensions . . . . .	31
4.3	Construction of 4-D Constellations having $D_4$ Lattice Structure . . . . .	31
4.3.1	$D_4$ with Spherical Boundaries . . . . .	32
4.3.2	Set Partitioning of a 4-D Cubic Constellation . . . . .	33
4.3.3	Union of Two 4-D Cubical Constellation . . . . .	33
<b>5</b>	<b>Performance and Detection of 4-D Modulations</b>	<b>36</b>
5.1	Asymptotic Power Efficiency and Spectral Efficiency . . . . .	36
5.2	Non Asymptotic Performance in AWGN Channel . . . . .	41
5.3	Constrained Capacity Curves . . . . .	48
5.3.1	Constrained Capacity in AWGN Channel . . . . .	48
5.3.2	Constrained Capacity in Partially Coherent AWGN Channel . . . . .	49
5.4	Detector Complexity . . . . .	50
5.4.1	Detection of 2-D Constellations . . . . .	50
5.4.2	Detector for $D_4$ Constellations Based on Set Partitioning Principle . . . . .	51
5.4.3	Alternate Detector for $D_4$ constellation . . . . .	52
5.5	Synchronization . . . . .	53
<b>6</b>	<b>Eight-Dimensional Joint Modulation Formats</b>	<b>56</b>
6.1	Eight Dimensional Packing Structures . . . . .	56
6.1.1	$Z_8$ -QAM . . . . .	56
6.1.2	$D_8$ -QAM . . . . .	57
6.1.3	$E_8$ -QAM . . . . .	57
6.2	Selected 8-D Modulations . . . . .	57
6.2.1	128- $D_8$ -QPSK . . . . .	57
6.2.2	256- $E_8$ -QAM . . . . .	58
6.3	Performance of 8-D Modulation Formats . . . . .	58
6.3.1	Asymptotic Power Efficiency and Spectral Efficiency . . . . .	59
6.3.2	Non Asymptotic Performance in AWGN Channel . . . . .	61
6.3.3	Constrained Capacity in AWGN and PC-AWGN Channel . . . . .	62
6.4	Detection of 8-D Modulations . . . . .	63
6.4.1	Detector for $D_8$ -QAM Constellation Based on Set Partitioning Method . . . . .	63
6.4.2	Detector for $E_8$ -QAM Constellations . . . . .	64
<b>7</b>	<b>Conclusion and Future work</b>	<b>67</b>
	<b>Appendix</b>	<b>70</b>
<b>A</b>	<b>Union Bound for Theoretical Symbol Error Rate</b>	<b>70</b>

<b>B</b>	<b>Constrained Capacity Curves in PC-AWGN channel</b>	<b>72</b>
----------	---	-----------



# List of Figures

2.1	Block diagram of a basic communication system. . . . .	4
2.2	Polarization components of the electric field in an electromagnetic wave . . . . .	8
2.3	A schematic view of a $2 \times 2$ LoS MIMO system. . . . .	9
2.4	Tx and Rx antennas arranged in an array . . . . .	9
2.5	Separating the signal stream in a $2 \times 2$ LoS MIMO . . . . .	11
2.6	Block diagram showing a design for cross polarization interference cancellation. . . . .	12
3.1	16-QAM constellation . . . . .	14
3.2	Receiver sensitivity of 4, 16 and 64-QAM at $\text{SER} = 10^{-7}$ . . . . .	16
3.3	BPSK constellation showing the pdf of a received symbol . . . . .	18
3.4	Diagram showing a QPSK constellation and the decision boundaries. . . . .	18
3.5	The probability distribution of the received QPSK symbols at high SNRs and its top view . . . . .	19
3.6	16-QAM with constellation points replaced by circles. . . . .	20
3.7	Standard 256-QAM and 256-Sph-QAM having circular boundary . . . . .	21
3.8	Hexagonal modulation format with circular boundaries having $A_2$ lattice structure. . . . .	22
3.9	Dense packing structure in three dimensions having HCP structure. . . . .	22
3.10	Asymptotic performance comparison of 2-D modulations . . . . .	23
3.11	Spectral efficiency vs. receiver sensitivity of 2-D modulations at $\text{SER} = 10^{-7}$ . . . . .	24
4.1	Dual polarized system viewed as two separate streams for communication . . . . .	26
4.2	Dual polarized system viewed as a single stream . . . . .	27
4.3	The QPSK constellation before and after inserting the new symbol in the void space . . . . .	28
4.4	The 3-D cubic constellation before and after inserting the new symbol in the void space . . . . .	29
4.5	Graphs showing the volume of the empty space and the radius of the sphere that can be inserted with the increase in dimension . . . . .	30
4.6	Projection of $2^{17}$ -Sph- $D_4$ constellation on horizontal and vertical polarization planes . . . . .	32

4.7	2-D analogy of set partitioning for construction of $D_4$ constellations from cubic constellation . . . . .	33
4.8	2-D analogy of construction of $D_4$ constellations using a cubic constellation and its shifted version. . . . .	34
5.1	Spectral efficiency vs. 1/PE plot for DP-QAM and SP-QAM constellation.	38
5.2	Spectral efficiency vs. 1/PE plot for DP-QAM and Sph- $D_4$ constellations.	39
5.3	PE/PE <sub>PAM</sub> vs. Spectral efficiency plot for four-dimensional modulations .	40
5.4	Packing density vs. spectral efficiency for SP-QAM modulations. . . . .	40
5.5	The nearest neighbour approximation SER curves of SP-QAM A modulation formats. . . . .	42
5.6	The nearest neighbour approximation SER curves of SP-QAM B modulation formats. . . . .	43
5.7	SER vs. SNR curves for selected SP-QAM constellations . . . . .	44
5.8	Spectral efficiency vs. receiver sensitivity at SER = $10^{-7}$ for SP-QAM and DP-QAM . . . . .	45
5.9	Spectral efficiency vs. receiver sensitivity for $2^{13}$ -SP-QAM and $2^{12}$ -DP-QAM at SER = $10^{-7}$ . . . . .	46
5.10	Spectral efficiency vs. receiver sensitivity for middle order SP-QAM and DP-QAM constellations at SER = $10^{-20}$ . . . . .	47
5.11	Constrained capacity curves for DP-QAM and SP-QAM constellations in AWGN channel. . . . .	49
5.12	Constrained capacity curves for DP-QAM and SP-QAM constellations in PC-AWGN channel . . . . .	50
5.13	16-QAM constellation with Voronoi regions of the constellation points. . .	51
5.14	2-D hexagonal constellation with Voronoi regions of the constellation points.	51
5.15	Schematic diagram showing the low complexity detector algorithm based on set partitioning. . . . .	52
5.16	Schematic diagram of low complexity detector for SP-QAM modulation formats. . . . .	53
5.17	Schematic view of synchronization using frame alignment word . . . . .	55
6.1	Spectral efficiency vs. 1/PE plot for 8-D modulations. . . . .	59
6.2	PE/PE <sub>PAM</sub> vs. spectral efficiency plot for eight-dimensional modulations	60
6.3	Packing density of $E_8$ -QAM and $D_8$ -QAM modulation formats with spectral efficiency. . . . .	61
6.4	SER vs. SNR plots of 8-D modulation formats. . . . .	62
6.5	Constrained capacity curves for 8-D modulations in AWGN channel. . . .	63
6.6	Block diagram showing the construction and detection of $E_8$ -QAM constellation. . . . .	65
6.7	Cross over SNR of two arbitrary modulation formats MOD-A and MOD-B having same SE. . . . .	66
A.1	Two adjacent constellation points considered for calculating $P_{\text{pep}}$ . . . . .	71

# List of Tables

5.1	Comparison between selected DP-QAM and $D_4$ constellations . . . . .	37
5.2	Comparison between Sph-DP-QAM and Sph- $D_4$ constellation . . . . .	37
5.3	Nearest neighbour multiplicity table for SP-QAM A constellations . . . . .	42
5.4	Nearest neighbour multiplicity table for SP-QAM B constellations . . . . .	42
6.1	Number of neighbours in 256- $E_8$ -QAM constellation. . . . .	58
6.2	Asymptotic power efficiencies of selected 8-D modulation formats with PS-QPSK. . . . .	59

# Notation

## Abbreviations

AWGN	Additive White Gaussian Noise
BER	Bit Error Rate
bps	Bits per second
DOF	Degree of Freedom
DP	Dual Polarized
DP-QAM	Dual Polarized Quadrature Amplitude Modulation
FAW	Frame Alignment Word
HSPA	High Speed Packet Access
IEEE	The Institute of Electrical and Electronics Engineers
ISI	Intersymbol Interference
LoS	Line of Sight
LTE	Long Term Evolution
MIMO	Multiple Input Multiple Output
ML	Maximum Likelihood
$N$ -D	$N$ -dimensions or $N$ -dimensional
PAM	Pulse Amplitude Modulation
PC-AWGN	Partially Coherent-Additive White Gaussian Noise
pdf	probability density function
PE	Asymptotic Power Efficiency
PSD	Power Spectral Density
PSK	Phase Shift Keying
PS-QPSK	Polarization Switched QPSK
QAM	Quadrature Amplitude Modulation
QPSK	Quadrature Phase Shift Keying
Rx	Receiver
SE	Spectral Efficiency
SER	Symbol Error Rate
SISO	Single Input Single Output
SNR	Signal to Noise Ratio
SP	Single Polarized
SP-QAM A	Set Partitioned QAM based on set partitioning method
SP-QAM B	Set Partitioned QAM based on shifting method

---

SS	Spatially Separated
TQAM	Triangular QAM or Hexagonal QAM
Tx	Transmitter
WiMAX	Worldwide Interoperability for Microwave Access
XPD	Cross-Polarization Discrimination
XPIC	Cross-Polarization Interference Cancellation

## Symbols

$\omega$	Angular frequency
$\mathbf{H}$	MIMO channel matrix
$B_c$	Coherence bandwidth
$B$	Signal bandwidth
$C$	Capacity
$d_R$	Rx antenna separation
$d_T$	Tx antenna separation
$E_b$	Average bit energy
$E_s$	Average symbol energy
$G$	Antenna gain
$M$	Number of levels or constellation points in $M$ -ary modulation
$M_a$	Number of receiver antennas in an antenna array
$N$	Number of dimensions
$N_a$	Number of transmitter antennas in an antenna array
$P(t)$	Pulse shaping filter
$p_X(x)$	Probability density function of random variable X
$P_b$	Bit Error Rate
$P_t$	Transmitted power
$P_r$	Received power
$P_{\text{pep}}$	Pair-wise Error Probability
$r$	Received symbol
$c$	Transmitted symbol or constellation point
$T_c$	Coherence time
$T_s$	Symbol period
$w$	Additive white Gaussian noise or distortion

## Lattice structures

$A_2$	Hexagonal lattice in two dimensions
$D_3$	The densest packing structure known in three dimensions
$D_4$	The densest packing structure known in four dimensions
$D_8$	A lattice structure in eight dimensions
$E_8$	The densest packing structure known in eight dimensions

$Z_N$       The cubic lattice in  $N$  dimensions

### Operators

$(\cdot)^T$       Transpose  
 $(\cdot)^*$       Complex conjugate transpose (Hermitian transpose)  
 $\delta(\cdot)$       Dirac-delta function  
 $\Re\{\cdot\}$       Real-part operator  
 $\Im\{\cdot\}$       Imaginary-part operator  
 $E[\cdot]$       Expectation value operator  
 $R(\cdot)$       Autocorrelation function

# Chapter 1

## Introduction

### 1.1 Background

The demand for high data rates for mobile devices has been growing rapidly. With the huge influx of mobile devices supporting high definition video, data intensive applications and them relying on clouds for both storage and processing, the demand for wireless broadband data is going to grow many folds. Although the technologies such as High Speed Packet Access (HSPA) and Long Term Evolution (LTE) have equipped the mobile devices with broadband data they have created tougher requirements on the capacity of the backhaul networks. Backhaul networks consist of links that connect base stations to network controllers. The base stations are often inaccessible to fiber solutions and also their installation is time consuming. A microwave line-of-sight (LoS) radio link that offers high data rates is thus a commonly used solution. The throughput of these links have to keep up with the increasing demands without requiring more spectrum.

The technologies such as cross polarization interference cancellation (XPIC) and LoS Multiple Input Multiple Output (MIMO) have enhanced the spectral efficiency to a large extent. A significant enhancement in spectral efficiency has been achieved from these technologies. Any possible techniques to further improve the spectral efficiency and exploit the potential of the expensive spectrum have to be considered. Dual polarization-multiplexing and spatially-separated LoS MIMO techniques have given rise to parallel streams for communication. The existing systems modulate and demodulate these parallel streams independently. However, it has been shown in optical communication that joint processing of two polarizations leads to power efficient modulations [1]. Similarly, the possibility of increase in spectral efficiency by employing joint processing of two polarizations has to be considered.

#### 1.1.1 Four-dimensional modulation

The LoS MIMO and Dual Polarization Multiplexing techniques have been studied extensively in literature. The advances in signal processing techniques have further made these techniques realizable. The principle behind the LoS MIMO is that the signal streams

are made orthogonal to each other by spatially separating the antennas at transmitter and receiver. Design of the antenna array and relation between the geometry of the antenna array and frequency of operation has been studied in literature [2, 3]. Dual polarization multiplexing allows the use of same bandwidth by both horizontal and vertical polarizations; the technique to reduce the leakage between the polarizations to make them orthogonal known as cross polarization interference cancellation has been discussed in [4, 5, 6] .

Dual polarization multiplexing and spatial separation techniques give rise to four and higher dimensional signal space. Attempts to utilize the higher dimensional space and hence the higher degrees of freedom have been made previously [7, 8, 9]. Lower order constellations in 4-D space have been investigated in terms of their SER performances [7]. Recently it has been shown that in optical coherent systems a considerable gain can be achieved by optimally modulating the 4-D signal space, the modulation format making use of 4-D signal space having better power efficiency than BPSK has been discussed [10]. The format PS-QPSK (Polarization Switched-QPSK) with 8 symbols in four Degree of Freedom (DOF) gives an asymptotic gain of +1.76dB with respect to BPSK and there have been experimental realizations of the format [11]. These works give a strong motivation to consider the joint modulation formats for microwave links which support dual polarization multiplexing.

The previous works on joint modulation formats in 4-D have concentrated on lower order constellations and mainly on optical communication for achieving power efficiency. Since the microwave LoS systems require high data rates, higher order joint modulation formats have to be considered. Recently the joint modulation formats in 4-D have been generalized and extended to higher order constellations having higher spectral efficiencies [12]. The study of higher dimensional modulations poses many challenges, the first being the difficulty in visualizing the higher order constellations in higher dimensions. The design and study of higher dimensional constellations also requires the concepts of lattices and sphere packing. The sphere packing problems are computationally complex and time consuming [10].

## 1.2 Problem Description

The goal of the thesis is to examine the joint modulation and detection of two polarization signals for higher order constellations and study the respective gains and losses. The joint processing results in four-dimensional signal space and different modulation formats in four dimensions were studied. Spectrally efficient modulations in four dimensions were discussed in detail and compared to other modulation formats. Two low complexity detectors were also analysed. Further, a few selected eight-dimensional joint modulation formats were evaluated in terms of power and spectral efficiency.



## **1.3 Thesis Organization**

Chapter 1 gives an overview of the problem under study and the work carried out. Chapter 2 is an overview of the wireless microwave systems and LoS microwave systems. Chapter 3 discusses the parameters related to modulation formats and defines the performance measures. Chapter 4 begins with the four-dimensional view of the dual polarization systems and introduces spectrally efficient modulations. Chapter 5 is dedicated to examining the performance of spectrally efficient joint modulation and comparing with other modulations. Detector complexity being a critical factor, it is also discussed for the introduced modulation formats in this chapter. A few selected joint eight-dimensional constellations are discussed in Chapter 6. Finally, Chapter 7 summarizes the results and discusses the scope of future work.

## Chapter 2

# Wireless Microwave Systems

This chapter gives a basic overview of wireless digital communication systems and LoS microwave systems.

Communication devices have evolved into highly complex systems supporting communication in adverse environments or channels. Though the systems have become highly complex, the basic design and operation principles have remained the same. This chapter gives a high level picture of these principles and the factors affecting such communication systems. Following which, LoS microwave communication systems are discussed in detail as this thesis aims to improve the performance of such systems.

### 2.1 Shannon Communication System Model

Communication systems can be best described on an abstract level by the Shannon model, Figure 2.1 shows the block diagram of a communication system [13].

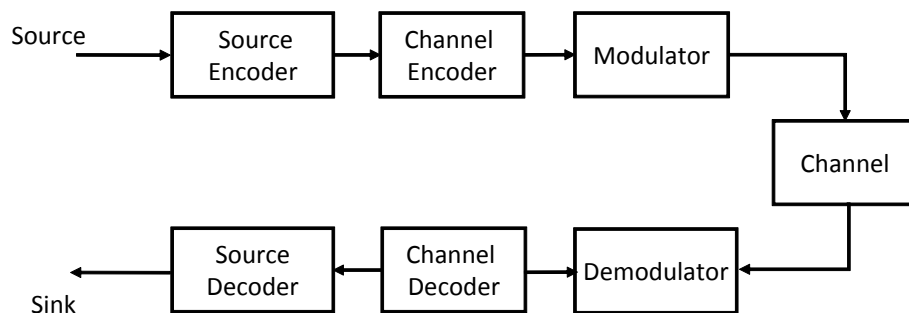


Figure 2.1: Block diagram of a basic communication system.

The source encoder encodes the data from the source into suitable digital format and reduces the redundancy in the data. This source coded data is then fed to the channel encoder. The purpose of the channel encoder is to add redundancy to the data to facilitate the receiver to reduce the number of errors introduced in the channel.

The modulator block is made up of several sub-blocks, most importantly bit to symbol mapper, pulse shaping and mixers. Bit to symbol mapper maps the bit sequence into symbols in  $M$ -ary modulation, the  $k$  coded bits are transformed using  $M = 2^k$  distinct symbols  $c_m, m = 0 \dots M-1$ . Common modulation formats are Phase shift keying (PSK), Frequency shift keying (FSK), Amplitude shift keying (ASK) and Amplitude phase shift keying (APSK). The pulse shaping filter maps the symbols to a sequence of pulses, the primary purpose of pulse shaping is to fix the shape and limit the bandwidth of the signal which shares a channel with other signals. The mixer up-converts the signal from baseband to passband frequencies. The modulated signal is passed through the channel which adds noise and interference to the transmitted signal.

At the receiver, each block undoes the operation performed by the corresponding block at the transmitter. The down-converted signal is filtered through a matched filter to minimize the effect of noise followed by sampling. The sampled signal is then passed through symbol to bit mapper, channel and source decoders. The block diagram gives a traditional design of a communication system, advances in communication theory allow interaction between coding and modulator to improve performance [13, pp. 3].

## 2.2 Channel Model

The channel is defined as the path over which the electrical signal traverses between the transmitter to receiver. It can be wired (e.g., copper, optical fibre) or wireless. The accessible to all and ever changing nature of our environment makes wireless channel more error prone to interference and highly time varying when compared to wired channel. The channel can introduce noise, interference from other signals (e.g., inter channel interference), inter symbol interference (ISI) and fading to the transmitted signal. Some of these aspects are discussed in the following sections.

### 2.2.1 AWGN channel

A common model for noise is *additive white Gaussian noise* (AWGN). It approximates many noises such as thermal noise and shot noise sources. It is called additive because it is additive in nature and white because it is uncorrelated or it has flat power spectral density. It is Gaussian because its real and imaginary parts follow the Gaussian probability density function. A continuous time complex baseband signal affected by complex AWGN is modeled as

$$r(t) = s(t) + w(t), \tag{2.1}$$

where  $s(t)$  is the input complex baseband signal,  $w(t)$  is the additive complex AWGN and  $r(t)$  is the received complex signal.

The autocorrelation function of AWGN is given by

$$R_w(t_1, t_2) = \frac{N_0}{2} \delta(t_1 - t_2),$$

where  $\delta(\cdot)$  is the Dirac-delta function,  $t_1, t_2$  are any two time instances and  $\frac{N_0}{2}$  is the one sided PSD of the AWGN.

### 2.2.2 PC-AWGN channel

*Phase noise* is another noise source and it mainly originates in the mixers that include oscillators. Ideally the oscillators have to generate a perfect sinusoid, but in reality the output has a random phase and amplitude fluctuation. The effect of phase noise on the sinusoid can be expressed as [14]

$$r(t) = A[1 + a(t)] \cos(\omega_c t + \theta(t)),$$

where  $A$  is the amplitude of the sinusoid,  $a(t)$  is the amplitude noise,  $\omega_c$  is the carrier angular frequency and  $\theta(t)$  is the phase noise. The phase noise rotates the signal constellation and it can completely ruin the reception if left untreated. In the frequency domain, phase noise appears as spectral widening.

Partially coherent AWGN channel (PC-AWGN) is a channel model where the signal is affected by both phase and AWGN noise. The complex baseband received signal has the form

$$r(t) = s(t)e^{j\theta(t)} + w(t),$$

where  $s(t)$  is the transmitted complex baseband signal;  $w(t)$  is the complex AWGN and  $\theta(t)$  is the phase noise. Phase noise can be modelled by different probability distributions, the common distribution models for phase noise are wrapped Gaussian and Tikhonov [15, 16]. Tikhonov-distributed phase noise closely models the residual phase noise when a phase-locked loop is used at the receiver [16].

The pdf of the Tikhonov distributed phase noise is given by

$$p_{\Theta}(\theta) = \begin{cases} \frac{e^{\rho \cos(\theta)}}{2\pi I_0(\rho)}, & \text{if } \theta \in [-\pi, \pi] \\ 0, & \text{if } \theta \notin [-\pi, \pi] \end{cases},$$

where  $\rho$  is a parameter of the Tikhonov distribution and is related to the variance of the angle  $\theta$  as  $\rho \propto \frac{1}{\sigma_{\theta}^2}$ .  $I_0(\rho)$  is the zero order Bessel function of first kind.

### 2.2.3 Fading

An important characteristic of the wireless channels is the multipath effect in which the transmitted signal reaches the receiver along multiple paths. The reflections and scattering cause the transmitted signal to be received in a number of copies each with its own phase delay and signal strength. The combination of multiple copies can be constructive or destructive resulting in a time varying signal to noise ratio at the receiver. The Fourier transform of the channel impulse response gives the response of the channel at different frequencies.

If the frequencies within the signal bandwidth  $B$  are discriminated significantly the channel is said to be frequency selective. The coherence bandwidth  $B_c$  is the bandwidth

for which the channel frequency response is considered to be flat. As a result a signal having a bandwidth  $B$  smaller than  $B_c$  experiences a near flat channel and if  $B$  is larger than  $B_c$  the signal experiences a frequency selective channel [17, Chapter 3].

The wireless channel being subjected to changing surroundings is also time varying. The changes in time are due to the relative motion between the transmitter-receiver or/and the changes in the environment. Coherence time  $T_c$  is a statistical measure of the time period over which the channel impulse response remains time invariant. If the symbol time  $T_s$  is smaller than  $T_c$ , the channel is said to be slow fading and if  $T_s$  is larger than  $T_c$  it is said to be fast fading since the channel impulse response changes within one symbol period [17, Chapter 3].

### 2.2.4 Intersymbol Interference

ISI is the overlapping of one or more adjacent or neighbouring symbols on a current received symbol. A symbol shifted in time will affect the neighbouring symbols. In wireless channels with multipath propagation, the symbols can arrive multiple times or/and shifted at receiver causing ISI. Symbol timing errors and non Nyquist filtering at transmitter and receiver can also cause ISI.

## 2.3 Microwave Systems

Due to increased shadowing by obstruction and attenuation, frequencies higher than 6 GHz are not used for mobile communication [18]. However, these frequencies are useful in LoS links. Another problem with high frequency communication is the path-loss, which increases with frequency as seen in [17, Eqn. 2.7]

$$\frac{P_t}{P_r} = \left( \frac{\sqrt{G}\lambda}{4\pi D} \right)^2, \quad (2.2)$$

where  $P_r$  and  $P_t$  are powers of received and transmitted signals, respectively.  $G$  is the product of transmitter and receiver antenna gains,  $D$  is the antenna separation and  $\lambda$  is the wavelength of the carrier.

Due to high attenuation and narrow frequency bands, mobile operators are considering microwave a bottle neck in capacity evolution. However by allowing microwave links to use new technologies such as LoS MIMO, dual polarized transmission along with the use of higher order modulation and newly available high frequency bands at 42 GHz and 70/80 GHz; it is possible to increase the capacity of microwave links up to 40 Gbps [19].

### 2.3.1 Dual Polarized Systems

Electromagnetic waves originate from the oscillation of electrical and magnetic fields which are orthogonal to each other. Electromagnetic wave travels in three-dimensional (3-D) space in a straight line perpendicular to electric and magnetic field. The electric field results from the voltage changes that occur as the antenna element is excited by an alternating waveform. The direction of the line of force of the electrical field is same as

the axis of the antenna. The magnetic field is a result of current flowing in the antenna and is perpendicular to the electrical field.

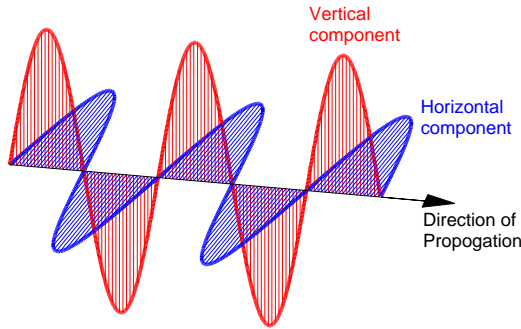


Figure 2.2: Polarization components of the electric field in an electromagnetic wave and its direction of propagation.

The polarization of electromagnetic waves indicates the plane in which the electrical field is vibrating (a convention). Since most waves of interest travel along the earth surface, often horizontal or vertical polarized waves is used, meaning the electrical field is oscillating in horizontal or vertical directions, respectively. The schematic diagram in Figure 2.2 shows the horizontal and vertical component of the electric field. The horizontal and vertically polarized signals being orthogonal to each other, can be regarded as two independent channels. A potential gain in spectral efficiency can be achieved by polarization multiplexing, meaning different data is sent in both polarizations using the same bandwidth.

In practical systems, due to imperfections in the channel and misalignment between antennas there is a leakage from one polarization to the other making two polarizations nearly orthogonal. This leakage can be quantified with channel cross-polarization discrimination factor (XPD). It measures the amount of power leaking from one polarization to another and thus measures the system's ability to differentiate between two polarizations. It is defined for vertical and horizontal components respectively as [20]

$$\text{XPD}_V = \frac{E[|h_{V,V}|^2]}{E[|h_{H,V}|^2]} \quad \text{XPD}_H = \frac{E[|h_{H,H}|^2]}{E[|h_{V,H}|^2]}, \quad (2.3)$$

where  $h_{A,B}$  is the channel impulse response from the  $A$  polarized Tx antenna to  $B$  polarized Rx antenna. Ideally  $|h_{H,V}|$  and  $|h_{V,H}|$  should be zero, meaning XPD is infinity. Higher the XPD is, higher the isolation between different polarizations.

### 2.3.2 LoS MIMO for Microwave Systems

MIMO is a promising technique that offers high data throughput by spatially multiplexing the signal stream, it offers diversity and array gain. A more detailed discussion on MIMO is available in [18].

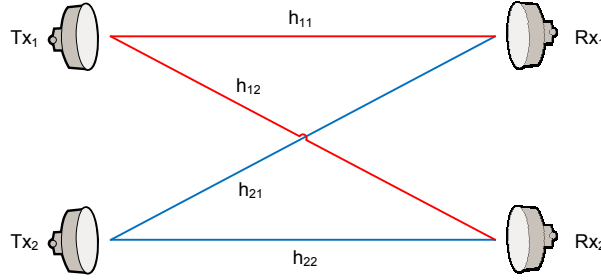


Figure 2.3: A schematic view of a  $2 \times 2$  LoS MIMO system.

A MIMO system in a rich scattering environment imposes low correlation between phase and amplitudes of received signals, meaning each received signal will experience independent paths. Consider two transmitter and two receiver antennas as shown in Figure 2.3. In case of a strong LoS component the correlation between the received signals increases further, by placing the antennas closely together the rank of the channel matrix becomes one. The MIMO system changes to a system identical to single input single output (SISO) system in capacity.

The channel gain  $h_{nm}$  between the  $n$ th transmitter antenna and  $m$ th receiver antenna is a function of geometry (the antenna separation distance and orientation) and carrier frequency. Since the phase of received signal depends upon the length of the path, one can intelligently set the distance between antennas and make signal streams near orthogonal. The principle behind LoS MIMO system is to make the signal streams orthogonal to each other, by spatially separating the antennas at the transmitter and receiver or/and by using orthogonally polarized antennas [14].

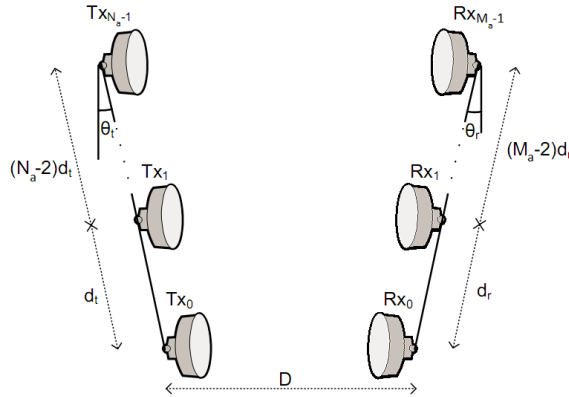


Figure 2.4: Tx and Rx antennas arranged in an array. The various distances and orientations are chosen optimally to make the signal streams orthogonal at the receiver.

Consider a uniform linear array of  $N_a$  transmitter and  $M_a$  receiver antennas separated by  $d_t$  and  $d_r$ , respectively, as shown in Figure 2.4. Optimal antenna separation providing

maximum capacity in LoS MIMO is given by [2, 14]

$$d_t d_r = \frac{\lambda D}{V \cos(\theta_t) \cos(\theta_r)} K, \quad (2.4)$$

where  $K$  is a positive odd integer normally chosen to be one, to obtain the smallest optimal antenna separation;  $D$  is the physical distance between Tx and Rx antenna arrays;  $\theta_t$  and  $\theta_r$  are tilt angles of Tx and Rx antennas, respectively;  $d_t$  and  $d_r$  are the transmitter and receiver antenna separations, respectively and  $V = \min(N_a, M_a)$ . It is seen from the above equation that, the separation between antenna decreases as the carrier frequency increases and it increases as the hop distance between Tx and Rx increases.

The channel matrix for a LoS MIMO system for a flat fading channel can be expressed as

$$\mathbf{H}_{\text{LoS}} = \begin{pmatrix} h_{11} & \cdots & h_{1M_a} \\ \vdots & \ddots & \vdots \\ h_{N_a 1} & \cdots & h_{N_a M_a} \end{pmatrix} = \begin{pmatrix} \exp(jkd_{11}) & \cdots & \exp(jkd_{1M_a}) \\ \vdots & \ddots & \vdots \\ \exp(jkd_{N_a 1}) & \cdots & \exp(jkd_{N_a M_a}) \end{pmatrix}, \quad (2.5)$$

where  $k = 2\pi/\lambda$  and  $d_{n_a m_a}$  is the physical distance between transmitter antenna  $n_a$  and receiver antenna  $m_a$ .

The concept of making the signals orthogonal by spatially separating the antennas at transmitter and receiver can be best explained by vector visualization. Consider a  $2 \times 2$  LoS MIMO system as in Figure 2.5 (courtesy [14]). As seen in Figure 2.5 a)-c) there is  $90^\circ$  phase difference between paths  $d_{11}$  and  $d_{12}$ . The receiver antennas Rx<sub>1</sub> and Rx<sub>2</sub> receive a signal that is a combination of transmitted signals from Tx<sub>1</sub> and Tx<sub>2</sub>. At the receiver, by rotating the received signals by  $-90^\circ$  and combining them, each signal stream can be detected without interference, even if the transmitted signals have different phases as shown in Figure 2.5 a)-c). The signal streams can also be separated when the phase difference between the paths is not  $90^\circ$  as shown in Figure 2.5 d).

### 2.3.3 Cross Polarization Interference Cancellation

The previous section described the leakage between the polarizations resulting in near orthogonal signals. For making use of the dual polarized systems as two separate streams the leakage has to be minimized.

Cross polarization interference cancellation is a digital signal processing technique that minimizes the leakage between the polarizations [4, 5, 6]. By minimizing the cross leakage, polarizations can be regarded as two independent streams and the capacity of the microwave links can be doubled by transmitting information simultaneously on both polarizations using the same frequency band. The channel for the dual polarized system can be viewed as a  $2 \times 2$  MIMO channel. Neglecting the phase differences between the Tx and Rx antennas the channel matrix can be written as



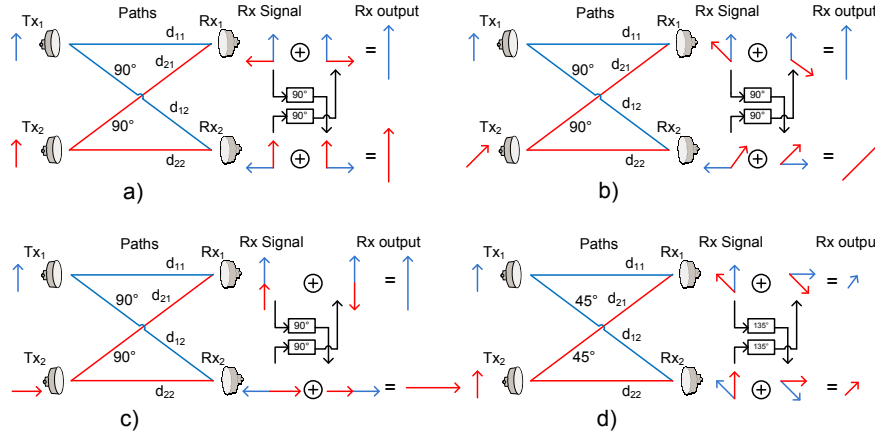


Figure 2.5: Separating the signal stream in a  $2 \times 2$  LoS MIMO. The figures a), b) and c) show how the signals at receiver can be made orthogonal to each other irrespective of their initial phases when the phase shift between the direct path and cross path is  $90^\circ$ . The figure d) shows the scenario when the phase difference between the direct path and cross path is not  $90^\circ$ . Copyright ©Haonan Liu and Tryggvi Ingason. Reprinted with permission from Haonan Liu and Tryggvi Ingason, can be found in [14].

$$\mathbf{W}_{XPD} = \begin{bmatrix} \sqrt{1-\alpha} & \sqrt{\alpha} \\ \sqrt{\alpha} & \sqrt{1-\alpha} \end{bmatrix}, \quad (2.6)$$

where  $\alpha$  is the channel gain between vertical transmitter and horizontal receiver antennas and vice-versa. It measures the ratio of power of one polarization that is transferred to other polarization and is constrained by  $0 \leq \alpha \leq 1$ . In terms of XPD it is defined as

$$\alpha = \frac{1}{XPD + 1}. \quad (2.7)$$

The advantage of dual polarized microwave links over spatially separated LoS link is that the antennas can be combined, thus there is no need to spatially separate the antennas at Tx and Rx. Block diagram of an XPIC system is shown in Figure 2.6. The receiver receives signals from both polarizations resulting in interference. XPIC filters the interference and subtracts the interference signal from the desired signal.

### 2.3.4 $4 \times 4$ SS DP LoS MIMO

Section 2.3.2 described the technique of spatially separating the Tx and Rx antennas to achieve near independent channels and Section 2.3.3 described XPIC to double the spectral efficiency using polarization multiplexing. Combining these two techniques results in a spatially separated dual polarized LoS MIMO (SS-DP LoS MIMO) system. This section describes the  $4 \times 4$  SS-DP LoS MIMO system which can produce 4 fold capacity

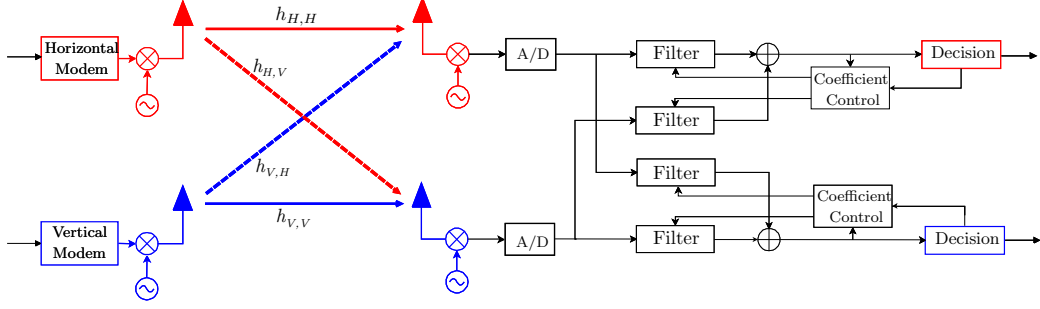


Figure 2.6: Block diagram showing a design for cross polarization interference cancellation.

in comparison to a SISO system. Combining Eqn. 2.5 and 2.6, the channel matrix for  $4 \times 4$  SS DP LoS MIMO can be written as [14]

$$\begin{aligned}
 \mathbf{H} &= \begin{bmatrix} h_{1V,1V} & h_{1V,1H} & h_{1V,2V} & h_{1V,2H} \\ h_{1H,1V} & h_{1H,1H} & h_{1H,2V} & h_{1H,2H} \\ h_{2V,1V} & h_{2V,1H} & h_{2V,2V} & h_{2V,2H} \\ h_{2H,1V} & h_{2H,1H} & h_{2H,2V} & h_{2H,2H} \end{bmatrix} = \begin{bmatrix} \mathbf{H}_{11} & \mathbf{H}_{12} \\ \mathbf{H}_{21} & \mathbf{H}_{22} \end{bmatrix} \\
 &= \begin{bmatrix} \sqrt{1-\alpha}e^{jkd_{11}} & \sqrt{\alpha}e^{jkd_{11}} & \sqrt{1-\alpha}e^{jkd_{12}} & \sqrt{\alpha}e^{jkd_{12}} \\ \alpha e^{jkd_{11}} & \sqrt{1-\alpha}e^{jkd_{11}} & \sqrt{\alpha}e^{jkd_{12}} & \sqrt{1-\alpha}e^{jkd_{12}} \\ \sqrt{1-\alpha}e^{jkd_{21}} & \sqrt{\alpha}e^{jkd_{21}} & \sqrt{1-\alpha}e^{jkd_{22}} & \sqrt{\alpha}e^{jkd_{22}} \\ \alpha e^{jkd_{21}} & \sqrt{1-\alpha}e^{jkd_{21}} & \sqrt{\alpha}e^{jkd_{22}} & \sqrt{1-\alpha}e^{jkd_{22}} \end{bmatrix}. \quad (2.8)
 \end{aligned}$$

Using the Kronecker product  $\otimes$ , the channel matrix can be expressed as

$$\mathbf{H} = \mathbf{H}_{\text{LoS}} \otimes \mathbf{W}_{XPD} = \begin{bmatrix} e^{jkd_{11}} & e^{jkd_{12}} \\ e^{jkd_{21}} & e^{jkd_{22}} \end{bmatrix} \otimes \begin{bmatrix} \sqrt{1-\alpha} & \sqrt{\alpha} \\ \sqrt{\alpha} & \sqrt{1-\alpha} \end{bmatrix}.$$

The channel matrix gives an insight into the inter-stream interference and the cross polarization interference. Efficient equalizers have to be designed to overcome these effects before feeding the signals to the detector. Design of algorithms for such MIMO space time equalizers have been discussed in detail in [14].

## Chapter 3

# Performance of Modulation Formats

Communication systems are used in diverse environments which affect the signals differently and have a direct effect on the performance of the system. The environment for a communication system is often described by the channel model whose characteristics were discussed in Chapter 2. The modulation format chosen and the channel have a direct consequence on the performance of the system. To obtain a desired performance, the modulation formats have to be subjected to scrutiny and comparison, keeping in consideration the channel they will be used on.

Though the diverse environments subject the signals to various kinds of noises and nonlinearities, AWGN is a prominent and a simple noise model generally chosen for measuring the performance of modulations. Though some other noises such as phase noise are critical in many systems, to keep the discussion simple this chapter considers the AWGN model only. Quality measures such as receiver sensitivity, spectral efficiency and power efficiency are used to compare different formats.

The performance of a modulation format is a direct consequence of its geometry. To understand the modulations which are already in use and the improved modulation formats which will be introduced in later chapters, understanding the relation between geometry and performance is important. Hence, this chapter discusses the importance of the geometry of the modulation formats.

### 3.1 Modulation Formats

The orthogonal components of the carrier in a coherent communication system facilitate a single carrier to carry two amplitudes, one on each orthogonal component and to be separated at the receiver. The two orthogonal components are referred to as in-phase ( $I$ ) and quadrature ( $Q$ ) components. The amplitudes can vary continuously, but they are chosen from a discrete set.

The pair of amplitudes form a symbol and owing to the fact that they are on orthogonal

### 3.1. MODULATION FORMATS

components. The symbol  $c_m$  is represented by a complex number as

$$c_m = I_m + iQ_m,$$

where  $I_m$  and  $Q_m$  are the amplitudes of the in-phase and quadrature components, respectively.

A modulation format is a set of such symbols  $C = \{c_1, c_2, \dots, c_M\}$  chosen appropriately to suit a communication system and channel. In a digital communication system, a sequence of complex symbols  $c[0], c[1], \dots, c[k]$  are taken from the finite alphabet set  $C$  at discrete time instances  $k$  and passed through a pulse shaping filter to form a complex continuous time baseband signal  $s(t)$ , which can be written as

$$s(t) = \sum_{k=0}^L c[k]v(t - kT_s), \quad (3.1)$$

where,  $v(t)$  is the pulse chosen and  $T_s$  is the symbol period.

Assuming that all the constellation points are chosen with equal probabilities,  $\log_2 M$  information bits are transmitted every symbol period  $T_s$ , yielding an information bit rate of  $R_B = (\log_2 M)/T_s$  bits per second (bps).

The modulation format making use of two orthogonal components can be visualized by 2-D Cartesian coordinates, in general a modulation format using  $N$ -orthogonal components can be visualized by  $N$ -dimensional Cartesian coordinates. Figure 3.1 shows the constellation diagram of 16-QAM (Quadrature Amplitude Modulation).

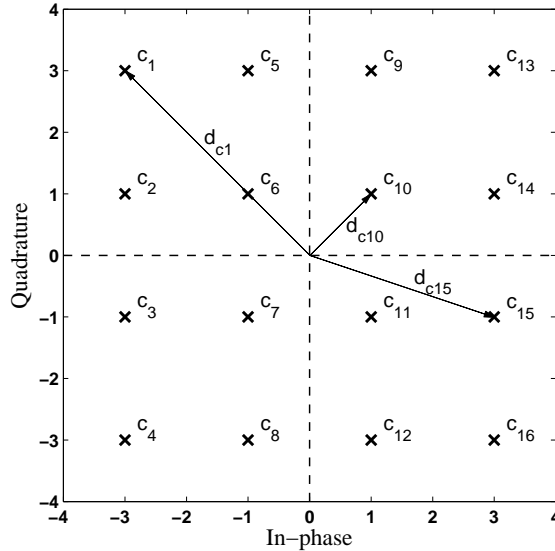


Figure 3.1: 16-QAM constellation. The figure shows the constellation points at different distances from the origin having different energies.

Since a modulation format is completely represented by its constellation plot in Euclidean coordinates, the term *constellation* is often used in place of modulation format in literature.

## 3.2 Definitions

### 3.2.1 Average Symbol Energy ( $E_s$ )

The energy of an alphabet or constellation point in a modulation format is equal to the square of the distance from origin to the point. In this definition the pulse shaping is assumed to be of unit energy. Figure 3.1 shows a simple modulation format. The distance from origin to the constellation point  $c_k$  is shown as  $d_{c_k}$ .

From the figure the energies of the constellation points are related as

$$\begin{aligned} E_{c_1} &= d_{c_1}^2 \\ E_{c_2} &= d_{c_2}^2 \\ &\vdots \\ E_{c_M} &= d_{c_M}^2. \end{aligned}$$

The average symbol energy of a modulation format or a constellation when the constellation points are equiprobable is given by

$$E_s = \frac{E_{c_1} + E_{c_2} + \dots + E_{c_M}}{M}. \quad (3.2)$$

Further, to compare the energy required by modulation formats with different number of bits per symbol, average bit energy  $E_b$  is used. The average bit energy is given by

$$E_b = \frac{E_s}{\log_2(M)}. \quad (3.3)$$

### 3.2.2 Symbol Error and Bit Error Rates

Symbol error rate (SER) is the ratio of number of symbols detected incorrectly to the number of transmitted symbols. Similarly, bit error rate (BER) is defined as the ratio of number of bits detected incorrectly to the number of transmitted bits. The relation between SER and BER is not always straight forward. In case of Gray mapping and at higher SNRs, they are approximately related as [17, Eqn. 5.47]

$$\text{BER} \approx \frac{\text{SER}}{\log_2 M}. \quad (3.4)$$

In constellations where Gray mapping is not possible the above approximation is not valid.

### 3.2.3 Receiver Sensitivity

Receiver sensitivity is defined as the signal to noise ratio required to reach a fixed BER or SER [13, pp. 133]. Figure 3.2 shows the procedure in which the receiver sensitivity is calculated. The signal to noise ratio  $E_b/N_0$  required to reach the SER of  $10^{-7}$  is determined as shown in Figure 3.2. The constellations 4-QAM, 16-QAM and 64-QAM have receiver sensitivities of 11.5 dB, 15.6 dB and 20.1 dB, respectively for  $\text{SER} = 10^{-7}$ . The SER plots in Figure 3.2 are obtained using the expression [21, Eqn. 45]

$$\text{SER} = 4 \left(1 - \frac{1}{\sqrt{M}}\right) Q \left( \sqrt{\frac{3(\log_2 M) E_b}{(M-1) N_0}} \right) - 4 \left(1 - \frac{1}{\sqrt{M}}\right)^2 Q^2 \left( \sqrt{\frac{3(\log_2 M) E_b}{(M-1) N_0}} \right),$$

where  $Q(\cdot)$  is the q-function.

The receiver sensitivity shows that, as the order of the constellation increases the SNR required to obtain a required performance also increases. It shows the trade-off between number of bits per symbol and the required power at a fixed performance.

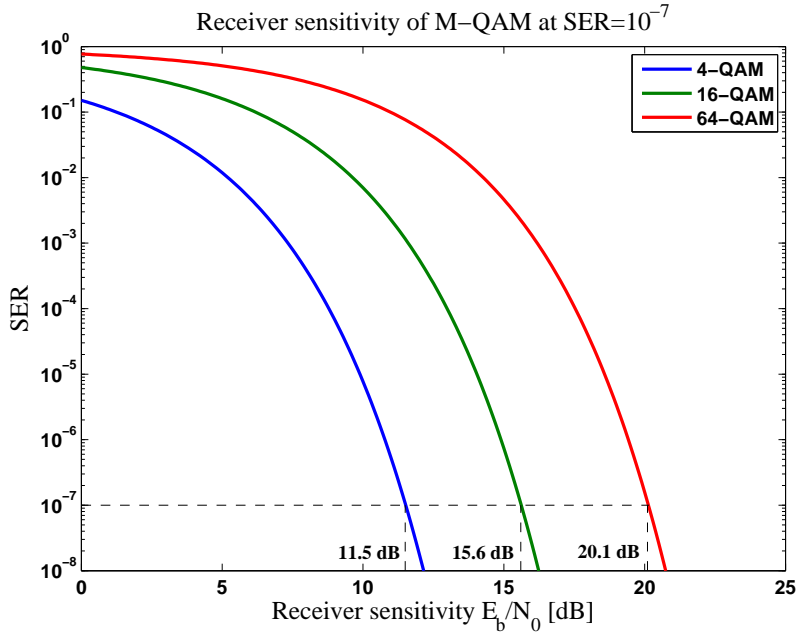


Figure 3.2: Receiver sensitivity of 4, 16 and 64-QAM at  $\text{SER} = 10^{-7}$ .

### 3.2.4 Spectral Efficiency

Spectral efficiency (SE) is the information bit-rate per bandwidth [bits/s/Hz] or information bits per *channel use*. Channel use refers to the use of a pair of  $I$  and  $Q$  components of a carrier. To simplify the definition we can assume the time equal to one symbol

### 3.3. CIRCLE APPROXIMATION OF A SYMBOL

---

period and bandwidth equal to 1 Hz. This would make the SE of modulation format to be bits/symbol. Further, to avoid confusion in dual polarization systems and higher dimensional systems, the definition is refined to

$$\begin{aligned} \text{SE} &= (\text{bits/symbol}) \text{ per polarization,} \\ \text{or SE} &= (\text{bits/symbol}) \text{ per channel use.} \end{aligned}$$

In the above definition the overhead and other redundancies introduced in communication systems are not considered.

#### 3.2.5 Asymptotic Power Efficiency

Let the distance between two constellation points  $c_k$  and  $c_l$  be denoted as  $d_{kl}$ , the minimum distance of the constellation is defined as  $d_{\min} = \min_{k,l} d_{kl}$ . The minimum distance  $d_{\min}$  between the constellation points is a critical parameter that affects the performance of a modulation format. The minimum distance and average symbol energy together are used to define asymptotic power efficiency (PE) as [22, pp. 220]

$$\text{PE} = \frac{d_{\min}^2 \log_2(M)}{4E_s}. \quad (3.5)$$

Asymptotic power efficiency is a relative measure of the power efficiency of the modulation format with respect to the Binary Phase Shift Keying (BPSK) constellation. For BPSK constellation the PE expression evaluates to 0 dB.

Note: Spectral efficiency or receiver sensitivity cannot be used separately to compare modulation formats fairly. A modulation format showing higher spectral efficiency could have poor receiver sensitivity and vice versa. As a consequence, ‘sensitivity and SE’ or ‘PE and SE’ have to be considered jointly for a fair comparison.

### 3.3 Circle Approximation of a Symbol

A symbol is represented by a point in the Cartesian co-ordinates as explained earlier. In this section an alternate way of representing symbols, that is representing a symbol by its circular territory is discussed. This representation is useful in understanding the performance of modulation formats.

Figure 3.3 shows a BPSK constellation with constellation points  $c_1$  and  $c_2$ . Consider the transmission of  $c_2$  over an AWGN channel, the sampled real received symbol can be written as  $r[k] = c_2 + w[k]$ ; where  $w[k]$  is the real AWGN sample. The probability distribution of the received symbol  $r[k]$  is Gaussian and has mean at  $c_2$ . If the symbols  $c_1$  and  $c_2$  are equiprobable, the midpoint of the line joining them specifies the decision region of the two symbols. The received symbol is detected as  $c_1$  if the received symbol crosses its decision region. The probability of symbol error i.e., the probability that  $c_2$

### 3.3. CIRCLE APPROXIMATION OF A SYMBOL

---

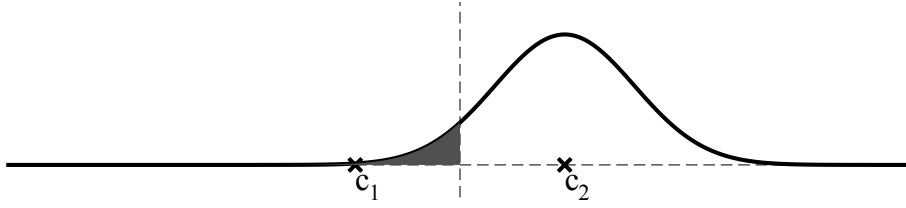


Figure 3.3: BPSK constellation showing the pdf of a received symbol when  $c_2$  is transmitted on AWGN channel.

is sent and  $c_1$  is detected is the area under the Gaussian curve from  $-\infty$  to 0 (shaded region in the figure). For a fixed variance of noise the distance between  $c_1$  and  $c_2$  can be determined to have a desired probability of error. And the regions separated by the midpoint can be regarded as the territories of the constellation points.

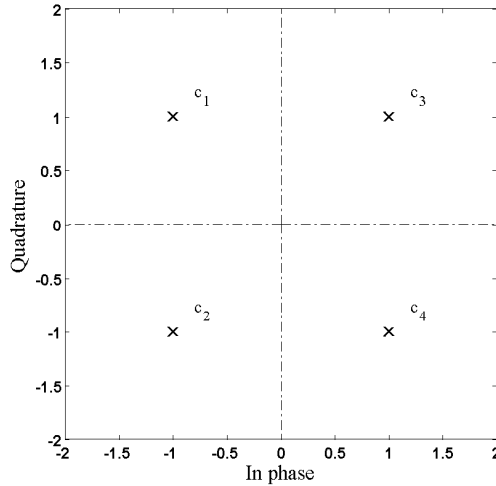


Figure 3.4: Diagram showing a QPSK constellation and the decision boundaries.

The idea of the territories of the constellation points can be understood clearly in 2-D modulation formats. Figure 3.4 shows a QPSK (quadrature phase shift keying) constellation. The dotted lines specify the decision regions of the constellation points. Consider the transmission of  $c_2$  over the AWGN channel. If the variance of the noise in both the in-phase and quadrature components is equal, the probability distribution of the sampled complex received symbol  $r[k] = c_2 + w[k]$  is an isotropic two-dimensional Gaussian with mean at  $c_2$ . The probability of detecting  $c_i, i \neq 2$  when  $c_2$  is transmitted i.e.,  $P(c_i|c_2), i \neq 2$  is equal to the volume of the 2-D Gaussian outside the decision region of  $c_2$ . For complicated constellations and constellations in many dimensions, this probability is difficult to compute as the decision regions have complex shapes. As a result the computation of SER for such constellation becomes complicated.

A simple and useful approximation to the SER is the union bound. It can be cal-



### 3.3. CIRCLE APPROXIMATION OF A SYMBOL

---

culated using pair-wise error probabilities, which are easy to calculate since they are functions of the distance  $d_{kl} = \|c_k - c_l\|$ . The union bound on SER can be expressed as [22, pp. 191]

$$\text{SER} \leq \frac{1}{M} \sum_{k=1}^M \sum_{\substack{j=1 \\ j \neq k}}^M \frac{1}{2} \text{erfc} \left( \frac{d_{kl}}{2\sqrt{N_0}} \right). \quad (3.6)$$

The term inside the summation represents the pair-wise error probability  $P_{\text{pep}}$  between the symbols  $c_k$  and  $c_l$ .

The bound is close to the actual SER at high SNRs and approaches the true SER asymptotically. It is clear from the equation that at high SNRs, SER is dominated by the set of points situated closely to each other. That is the points at a distance  $d_{\text{min}}$  from each other. From this observation it is clear that if a constellation is to be optimized to minimize the average symbol energy  $E_s$ , the  $d_{\text{min}}$  has to be kept unreduced to keep the SER performance unchanged (at high SNRs). The restriction of keeping the minimum distance unreduced while trying to minimize  $E_s$  and the isotropic nature of the noise allows us to replace the constellation points with non overlapping circles of diameter equal to the minimum distance. By not allowing the circles to overlap we ensure that the required  $d_{\text{min}}$  is guaranteed.

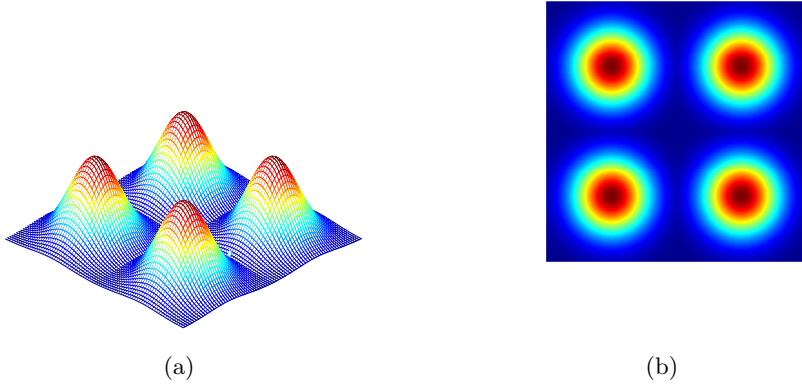


Figure 3.5: (a) The probability distribution of the received QPSK symbols at high SNRs (b) and its top view justifying the circle approximation of a constellation point.

Let us consider the probability distribution of the received symbols of the QPSK constellation at high SNRs as seen in Figure 3.5(a). Figure 3.5(b) shows the top view of the probability distribution, the top view supports the idea of replacing the constellation points by circles.

The above discussion leads to the conclusion that any constellation point in 2-D constellations can be replaced by a circle when transmission is on AWGN channel. Extending the argument to higher dimensions, in three-dimensional constellation a constel-

lation point can be replaced by a sphere and in  $N$  dimensions by an  $N$ -sphere<sup>1</sup>. The interpretation of symbols by their circular territories or spheres gives a useful insight into the performance of the modulations which is made clear in the following section.

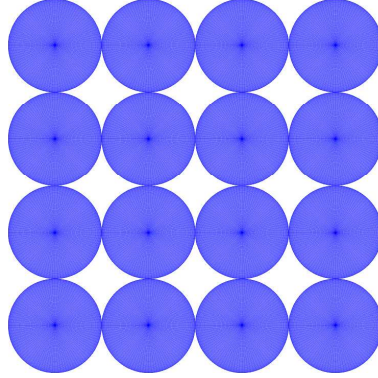


Figure 3.6: 16-QAM with constellation points replaced by circles.

In Figure 3.6, the constellation points of 16-QAM modulation format are replaced by circles of equal diameter (diameter equal to  $d_{\min}$ ). The minimum distance  $d_{\min}$  ensures the desired performance of the constellation at high SNRs. Void space in between the circles indicate excess energy being spent to achieve the desired performance. To reduce the consumption of this additional energy, the void space has to be reduced; this is achieved by rearranging the circles without overlap under the constraint that  $E_s$  is minimized.

The problem of finding the arrangement of 16 constellation points to minimize the average energy requirement is equivalent to finding the densest packing of 16 circles in two dimensions. Generalizing the statement the problem of finding the constellation with maximum asymptotic power efficiency is equivalent to finding the densest packing of  $M$   $N$ -dimensional spheres (Sphere packing problem) [10]. This is equivalent to finding an arrangement of  $N$ -spheres that minimizes the average squared distance of their centres from the origin.

The problem of finding the densest packing is challenging and no formal mathematical proofs are known. The best known packing structures obtained by empirical methods are used to define the most power efficient constellations in the sense that no better constellations have been found [23, pp. 228]. As the number of constellation points and dimensions increase the complexity of the problem of finding the densest packing grows and is computationally demanding.

#### Constellation with Circular Boundaries

The sphere packing problem solution for large number of spheres or constellation points results in constellation with spherical boundaries. This is due to the fact that the

---

<sup>1</sup>An  $N$ -sphere is a generalization of the surface of an ordinary sphere to arbitrary  $N$  dimensions.

### 3.4. POWER EFFICIENT MODULATION FORMATS IN TWO AND THREE DIMENSIONS

---

constellation packed densely and bounded by spherical boundaries has the least  $E_s$  and is the most power efficient. Also if there is a constraint on the packing arrangement, then for that packing arrangement the constellation with the spherical boundaries has higher power efficiency than the constellation with non spherical boundaries.

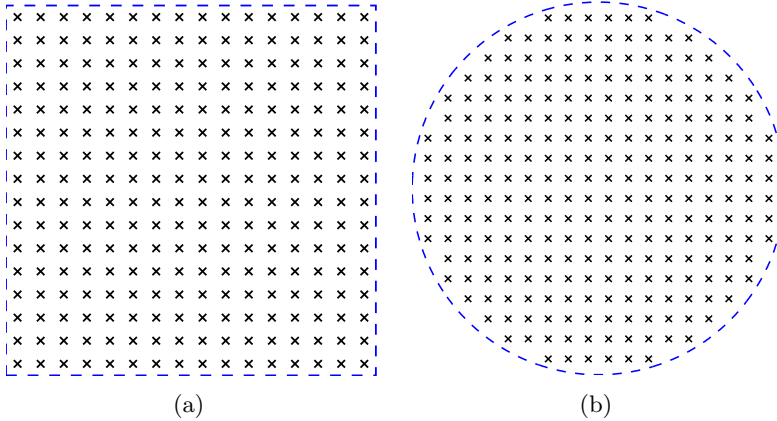


Figure 3.7: (a) Standard 256-QAM having rectangular boundary (b) 256-Sph-QAM having circular boundary. 256-Sph-QAM is more power efficient than 256-QAM due to shaping gain.

Consider the standard 256-QAM constellation and the constellation with 256 points having the same arrangement structure (i.e., cubic) and circular boundary which will be referred to as 256-Sph-QAM. Figures 3.7(a) and 3.7(b) show the two constellations considered.

The asymptotic power efficiencies of 256-QAM and 256-Sph-QAM are  $-13.2736$  dB and  $-13.0843$  dB, respectively. The values of power efficiencies are in support of the argument in the section. The increase in the power efficiency obtained by shaping the boundary is referred to as *shaping gain* ( $\gamma_s$ ). The maximum shaping gain that can be achieved in two dimensions is 0.2 dB [24, Table I], [25, Table I].

### 3.4 Power Efficient Modulation Formats in Two and Three Dimensions

In two dimensions, the hexagonal packing of circles is known to be the best packing structure and is known as  $A_2$  [26, Table 1.2]. Figure 3.8 shows the hexagonal constellation with 19 points which is bounded by a circular boundary. The dense hexagonal packing and the spherical boundary make the constellation the most power efficient modulation format known so far with 19 points in two dimensions [23]. Also, the hexagonal constellation arrangement is referred to as TQAM (triangular QAM) [27] as the points can be interpreted to be arranged on the vertices of contiguous equilateral triangles.

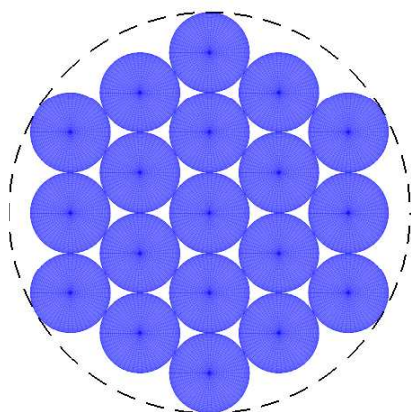


Figure 3.8: Hexagonal modulation format with circular boundaries having  $A_2$  lattice structure.

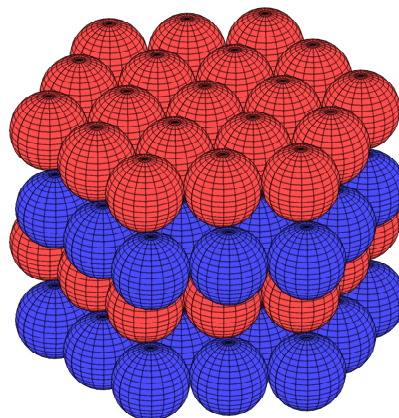


Figure 3.9: Dense packing structure in three dimensions having HCP structure.

Similarly, the densest known packing structures in three dimensions are Face-centered cubic (FCC) and Hexagonal close packing (HCP) [26, Table 1.2],[28]. The structure of HCP is shown in Figure 3.9, suitable modulation formats can be extracted from the extended structure by choosing  $M$ -ary cubical or spherical subsets. The packing structure is made up of three dimensional spheres arranged in hexagonal pattern in each layer. The detailed description of the construction of these structures can be found in [26].

### 3.4.1 Kissing Number

An important parameter of regular packing structures as shown in Figure 3.9 is the maximum number of nearest neighbours a point or a sphere has. In the 16-QAM constellation shown in Figure 3.6, a circle has a maximum of four nearest neighbours. The points in the hexagonal constellation and the dense 3-D structure shown in Figure 3.9 have a maximum of 6 and 12 neighbours, respectively [26, Table 1.2]. The maximum number of nearest neighbours a point has in a structure is known as *kissing number*.

The kissing number plays an important role in the SER performance of the constellations. In case of transmission over AWGN channel, the probability distribution of the received symbol has a mean at the transmitted constellation point and spreads around it as shown in the Figure 3.5(a). The number of neighbours closest to the point significantly affect the SER performance of the constellation as indicated by the Eqn. 3.6.

The probability that the received symbol is wrongly detected increases if the number of closest neighbours increases.

### 3.5 Comparison of Modulation Formats

The comparison of two modulation formats has to be fair, meaning all the important aspects of the modulation formats have to be considered. The number of bits per symbol, SER performance and the power required per bit have to be considered together for a fair comparison. This is important because a modulation format can have a better SER performance compared to another modulation, but it could have lower SE.

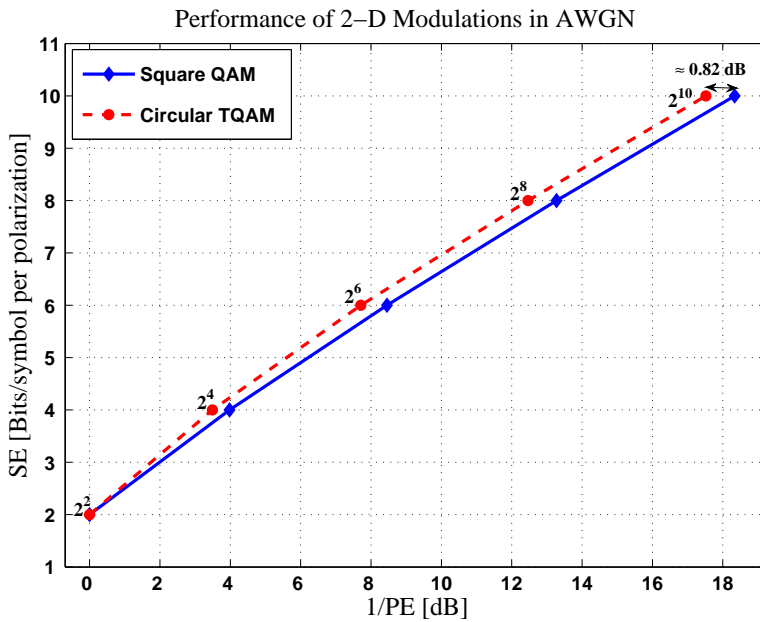


Figure 3.10: Asymptotic performance comparison of 2-D modulations. The graph shows the higher power efficiency of circular TQAM over QAM.

Figure 3.10 shows the plot of SE vs.  $1/PE$  for QAM and circular-TQAM constellations in AWGN. The circular TQAM constellations used to obtain the plot were formed by generating a large number of points arranged in hexagonal structure and then choosing a  $M$ -ary circular subset. The centroid of the subset is moved to origin to minimize the average symbol energy  $E_s$ . The constellations obtained from this procedure for small  $M$  are not optimal, the constellation from the circular subset are used directly and no optimizations have been done to generate the plot. Such plot is used to compare modulation formats in [10]. The points lying more towards left have higher asymptotic power efficiencies. For a fixed spectral efficiency the figure shows that the circular TQAM has higher asymptotic power efficiency when compared to QAM.

### 3.5. COMPARISON OF MODULATION FORMATS

A fair and common way to compare modulation formats is to represent a modulation format in spectral efficiency vs. sensitivity plane [10, 22]. In this scheme of comparison, the performance of the modulation formats i.e., SER or BER is fixed and the SNR required to achieve this performance is found. Since this comparison includes SNR (a measure of energy), performance (fixed SER or BER) and spectral efficiency it is a fair comparison for modulation formats. This scheme shows the ‘SE - sensitivity’ trade-off. For obtaining the sensitivities at a given SER, exact SER expressions can be used or union bounds which are close (tight at high SNR) to the exact SER curves at the specified SER can be used.

Figure 3.11 shows the SE vs. sensitivity plot for different QAM and PSK constellations. Consider the  $2^4$ -QAM and  $2^4$ -PSK constellations. From the plot it is clear that in AWGN,  $2^4$ -QAM has better sensitivity than  $2^4$ -PSK, as a consequence in AWGN channel  $2^4$ -QAM is chosen over  $2^4$ -PSK.

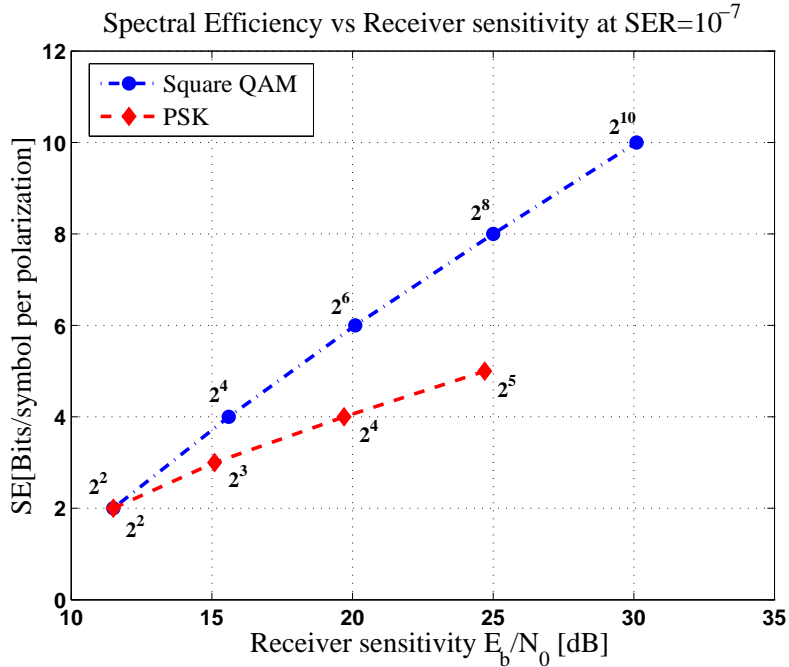


Figure 3.11: Spectral efficiency vs. receiver sensitivity of 2-D modulations at  $SER=10^{-7}$ .

## Summary

In this chapter the basic properties and a few important parameters of modulation formats were defined. The analogy of circles and spheres with the constellation points was discussed. Finally, two fair methods to compare the modulation formats were explained.

## Chapter 4

# Four-Dimensional Modulation Formats

The required isolation between the horizontal and vertical polarization in dual polarization systems is achieved by digital signal processing techniques as explained in Section 2.3.3. These advancements have enabled the use of both polarization components for data transmission in microwave communication. Dual polarization communication systems are commercially deployed in microwave LoS solutions [19].

This chapter looks into the details of the modulation formats used in the dual polarization systems.

### 4.1 Dual Polarization Multiplexing

Ideally the horizontal and vertical polarization components can be considered as two orthogonal components of the electromagnetic wave. But in practice they cannot be isolated completely; there is a leakage between the polarizations. As mentioned in Section 2.3.3 XPIC techniques have enabled the isolation of the polarizations to a great extent.

A dual output modem or two single output modems, modulate two separate bit streams independently and are connected to the vertical and horizontal polarization inputs of an antenna. At the receiver side, XPIC techniques are employed and the horizontal and vertical streams are processed separately. As a simple example, 16-QAM modulation format can be used in both the horizontal and vertical polarization.

There is a different way of looking at the dual polarization system. We now describe the basic properties of the electromagnetic field [9, 23] and how it can be interpreted as a four-dimensional signal. The electromagnetic field has two quadratures in two polarization components, thus in total four DOF. The electric field amplitude of the optical wave or microwave can be written as

$$E = \begin{pmatrix} E_{h,r} + iE_{h,j} \\ E_{v,r} + iE_{v,j} \end{pmatrix} = \begin{pmatrix} |E_h| \exp(i\psi_h) \\ |E_v| \exp(i\psi_v) \end{pmatrix}, \quad (4.1)$$

where  $h$  and  $v$  indicate the horizontal and vertical components,  $r$  and  $j$  the in-phase and orthogonal components, respectively. The phases  $\psi_h$  and  $\psi_v$  are in the interval of  $(-\pi, \pi]$  radian. The electric field can also be described in terms of its phase, amplitude and polarization state as

$$E = \|E\| \exp(i\psi_a) \begin{pmatrix} \cos(\theta) \exp(i\psi_r) \\ \sin(\theta) \exp(-i\psi_r) \end{pmatrix}, \quad (4.2)$$

where  $\|E\|^2 = \|E_h\|^2 + \|E_v\|^2$ ,  $\theta = \arcsin(\|E_v\|/\|E\|)$ , the absolute phase  $\psi_a = (\psi_h + \psi_v)/2$  and the relative phase  $\psi_r = (\psi_h - \psi_v)/2$  between the field polarization components. The relative phase  $\psi_r \in (-\pi, \pi]$  radian describes the ellipticity of the polarization state. The angle  $\theta \in [0, \pi/2]$  radian describes the orientation in the  $h$ - $v$  plane of the linear polarization state or the major axis of the polarization ellipse. The final and the most useful notation in relevance to the modulation formats is

$$s = \begin{pmatrix} E_{h,r} \\ E_{h,j} \\ E_{v,r} \\ E_{v,j} \end{pmatrix} = \begin{pmatrix} \|E\| \cos(\psi_h) \sin(\theta) \\ \|E\| \sin(\psi_h) \sin(\theta) \\ \|E\| \cos(\psi_v) \cos(\theta) \\ \|E\| \sin(\psi_v) \cos(\theta) \end{pmatrix}. \quad (4.3)$$

This notation gives a different perspective of the dual polarization communication system. The dual polarization systems have four degrees of freedom and hence instead of using two separate two dimension modulations, one four-dimensional modulation format can be used.

#### 4.1.1 Four-Dimensional view of Dual Polarized Systems

Figure 4.1 is a schematic diagram showing the use of horizontal and vertical polarizations as independent streams for communication. Separate 2-D QAM modulations are used in both polarizations and the detection is done independently.

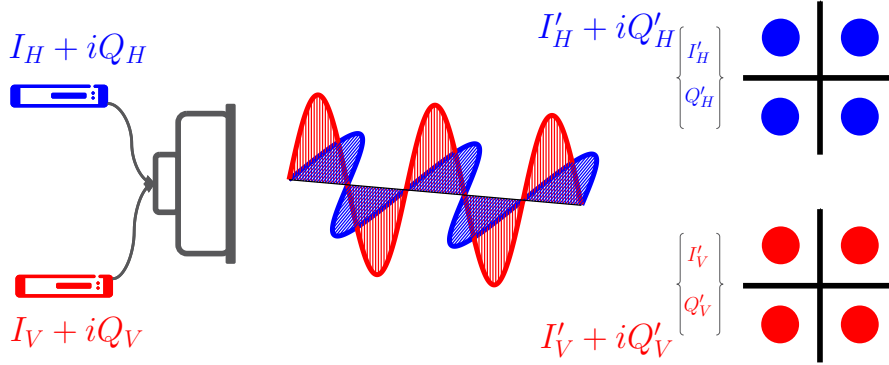


Figure 4.1: Dual polarized system viewed as two separate streams for communication. Each polarization allows a 2-D modulation format.

The dual polarization communication systems making use of  $M$ -QAM modulation formats in each polarization can also be viewed as using a four-dimensional modulation.



Figure 4.2 clarifies the idea. The resulting four-dimensional modulation format is referred to as Dual Polarized QAM (DP-QAM). The modulation format in four dimensions has  $M \times M$  constellation points and has a bit rate of  $(\log_2(M \times M))/T_s$ .

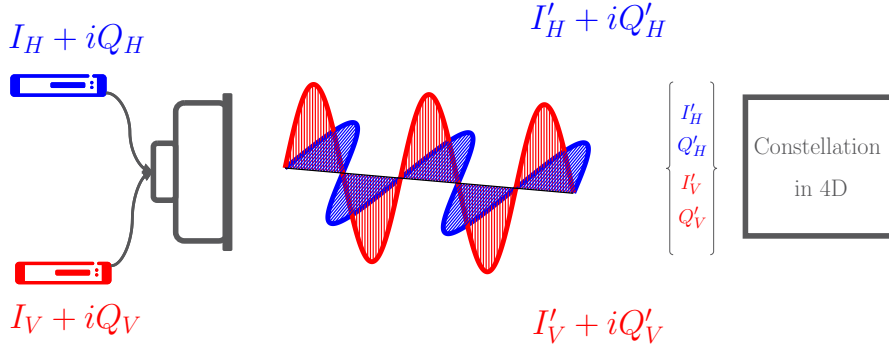


Figure 4.2: Dual polarized system viewed as single stream, both polarizations together allow a 4-D modulation format.

Consider, for example,  $(16 \times 16)$ -DP-QAM modulation format. The constellation points of DP-QAM now lie in four-dimensional Euclidean space. As described in Section 3.3, the constellation points can be replaced by four-dimensional spheres of equal radii and diameter equal to the minimum distance. Visualizing the four-dimensional constellation is not straight forward and it has to be done by considering the projection onto two and three dimensions. Consider the projection of the  $(16 \times 16)$ -DP-QAM on a plane formed by any two principal orthogonal dimensions for example on the plane formed by the in-phase and quadrature components of horizontal polarization component i.e.,  $E_{h,r}$ - $E_{h,j}$  plane. The projection is equivalent to 16-QAM as shown in Figure 3.6 and has a significant amount of void space. The void space indicates the inefficiency of the modulation in terms of power efficiency for a fixed desired performance. It is clear from the observation that though DP-QAM has twice the spectral efficiency in comparison to QAM in non-polarized system, it is not the most power efficient or optimum format in four dimensions and thus there is still potential for improvement.

## 4.2 Geometry of the Cubic Constellations

As suggested in Chapter 3, the problem of finding the most power efficient modulation in an  $N$ -dimensional space is equivalent to a sphere packing problem. Though this is the most logical and straightforward procedure, looking at the geometry and shortcomings of the cubic constellations (e.g., DP-QAMs) gives a good insight.

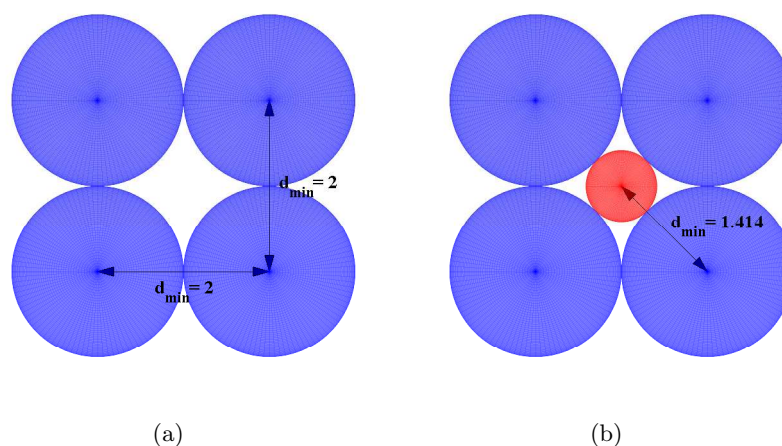


Figure 4.3: (a) QPSK constellation and (b) QPSK constellation after inserting the new symbol in the void space.

Figure 4.3(a) shows QPSK modulation format, cubic constellation in two dimensions. Let the circular symbols be of unit radius resulting in a minimum distance of 2 units, in vector notation the points can be written as  $([1,1], [1,-1], [-1,1], [-1,-1])$ . The void space in between the four symbols indicates that the format is non-optimal in terms of power efficiency. Consider inserting a new symbol in the void space without overlapping the existing four symbols. Figure 4.3(b) shows the newly inserted symbol at  $[0,0]$  and it has a radius of 0.414 units. Though the inserted symbol increases the average number of bits per symbol, the minimum distance of the constellation is now reduced from 2 units to 1.414 units. This reduction in minimum distance results in degradation of SER performance.

Extending the symbol insertion problem to three dimensions, the advantage of modulation formats in higher dimensions is seen clearly. Consider a cubic constellation in three dimensions, with constellation points located at the vertices of a cube of sides equal to 2 units. Figure 4.4(a) shows the 3-D cubic constellation with spherical symbols of unit radius resulting in a minimum distance of 2 units. One corner symbol has been removed to show the void space. In vector notation the points can be written as  $([-1,-1,-1], [-1,-1,1], [-1,1,-1], [-1,1,1], [1,-1,-1], [1,-1,1], [1,1,-1], [1,1,1])$ . Let us now insert a non overlapping sphere in the void space created by the eight spheres. Figure 4.4(b) shows the newly inserted sphere at  $[0,0,0]$  and it has a radius of 0.7321 units. The inserted symbol reduces the minimum distance of the format from 2 units to 1.7321 units. Again the number of bits per symbol has increased but at the cost of reduced minimum distance and hence reduced performance in terms of SER.

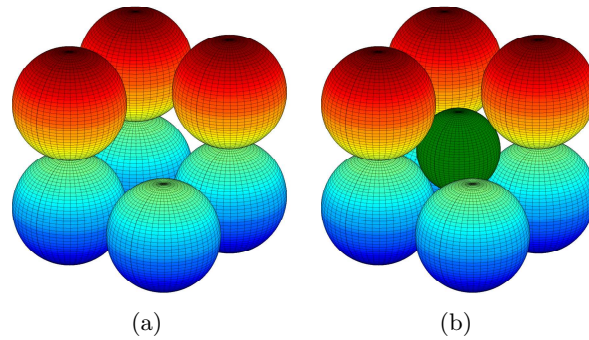
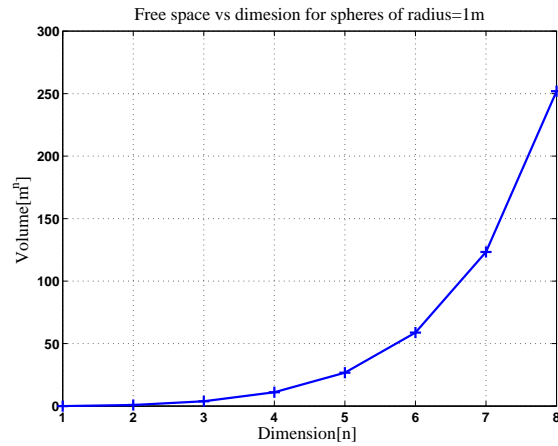
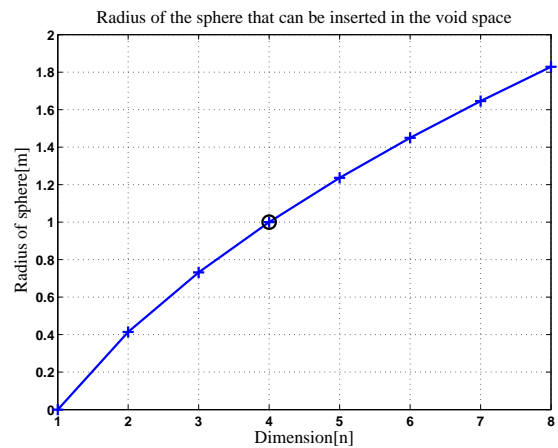


Figure 4.4: (a) The 3-D cubic constellation before and (b) after inserting the new symbol in the void space.

Generalizing the symbol insertion problem to  $N$  dimensions, the increase in the radius of the  $N$ -sphere that can be inserted with dimensions is computed. Figures 4.5(a) and 4.5(b) show the increase in the volume of the void space and the increase in the radius of the  $N$ -sphere that can be inserted in the void space with dimensions. With increase in dimension the volume of the void space increases exponentially and the radius of the inserted symbol increases near linearly.



(a)



(b)

Figure 4.5: Graphs showing (a) the volume of the empty space and (b) the radius of the sphere that can be inserted with the increase in dimension.

If the plot of radius with dimensions in Figure 4.5(b) is observed, the radius of the inserted  $N$ -sphere in 4-D is exactly equal to one. This implies that a non overlapping 4-sphere of unit radius can be inserted in the void space created by the 4-D cubic constellation. The minimum distance after the insertion of the new sphere/symbol is still 2 units, meaning that an increase in average number of bits per symbol is achieved without degradation in performance at higher SNRs (high SNR is relative to the order of the constellation, as an approximation SNRs corresponding to a SER of  $10^{-3}$  can be considered as high). We can conclude from these observations that the four-dimensional cubic constellation can be modified to increase the spectral efficiency without degrading the performance at high SNRs.

From the discussion in this section, it is evident that the spectral efficiency in dual

polarization communication systems can be improved without compromising the SER performance.

#### 4.2.1 A Spectrally Efficient Modulation in Four Dimensions

Consider the  $(16 \times 16)$ -DP-QAM constellation. To increase the number of bits per symbol by one, the number of constellation points has to be doubled. To double the number of symbols, the new symbols can be inserted in the void space present in the cubic constellation and the remaining symbols can be placed outside the boundaries of the 4-D cube. An easy way to generate this arrangement of points is to take the union of  $(16 \times 16)$ -DP-QAM four-dimensional cubic constellation and a shifted version of the same, shifted by the offset vector  $[\frac{d_{\min}}{2}, \frac{d_{\min}}{2}, \frac{d_{\min}}{2}, \frac{d_{\min}}{2}]$ . To minimize the average symbol energy, the centroid of the constellation points is calculated and the whole constellation is shifted to have centroid at origin. This results in a four-dimensional modulation format with  $(2 \times 16 \times 16)$  points retaining the same minimum distance as in  $(16 \times 16)$ -DP-QAM. There is a small increase in the energy requirement per bit due to the asymmetrical nature of the constellation about the origin. The performance of the constellation is discussed in detail in the next chapter.

The constructed modulation has better spectral efficiency than the DP-QAM constellation. However, it does not prove that the constructed modulation is the optimum (most power efficient) modulation format in 4-D. Finding the most power efficient modulation in  $N$  dimensions, is equivalent to finding the most dense packing structure of  $N$ -dimensional spheres. The densest known packing structure in four dimensions is the  $D_4$  lattice [26, Table 1.2] and one of the methods to construct the  $D_4$  lattice described in [29] is using a cubical lattice and its shifted version which resembles the procedure described in the previous paragraph. From this observation it can be concluded that the symbol insertion experiment in 4-D leads to the most dense packing structure  $D_4$  while also highlighting the shortcomings of the DP-QAM constellation.

Although  $D_4$  is the most dense packing structure in four dimensions, the number of points chosen for constructing the constellation and the shape of the boundary of the constellation has a significant impact on the average symbol energies. The efficient modulation formats constructed must also have a reasonable detector complexity to be applicable in high data rate communication systems.

### 4.3 Construction of 4-D Constellations having $D_4$ Lattice Structure

It is essential to know the methods in which  $D_4$  lattice structure is constructed, so that useful constellations from the structure can be extracted. The most simple approach to generate  $D_4$  lattice is from the integer lattice  $Z_4$ .  $Z_4$  is an integer lattice which is made up of a linear combination of integer multiples of the basis vectors  $[1 \ 0 \ 0 \ 0], [0 \ 1 \ 0 \ 0], [0 \ 0 \ 1 \ 0]$  and  $[0 \ 0 \ 0 \ 1]$ . The points in  $Z_4$  whose coordinates add to even numbers form  $D_4$ . The detailed definition and construction of  $D_4$  lattices can be found in [26].

### 4.3. CONSTRUCTION OF 4-D CONSTELLATIONS HAVING $D_4$ LATTICE STRUCTURE

---

This section describes three constructions having the  $D_4$  lattice structure, which are the most feasible arrangements as modulation formats owing to their regularity. To visualize the four-dimensional modulation formats on paper, the components of constellation on the horizontal ( $I_H$  and  $Q_H$  plane) and the vertical ( $I_V$  and  $Q_V$  plane) polarization planes are plotted separately. Although the separate plots completely misrepresent the structure in four dimensions, they are useful in visualizing the boundaries which are important characteristic of a modulation format.

#### 4.3.1 $D_4$ with Spherical Boundaries

For a given arrangement pattern and number of constellation points it is known that the constellation with the spherical boundaries has the highest power efficiency as described in Chapter 3. Similarly, by generating a large number of points arranged in  $D_4$  lattice structure and choosing an  $M$ -ary spherical subset enclosed by a sphere with center at origin, we obtain a  $M$ -spherical- $D_4$  ( $M$ -Sph- $D_4$ )<sup>1</sup> modulation format. The centroid of the subset is then moved to origin to minimize the average symbol energy  $E_s$ . When  $M$  is small this procedure could result in non optimal constellations and some reconfiguration of the outer points has to be made. For large  $M$  this procedure results in near optimum constellations. Figures 4.6(a) and 4.6(b) show the horizontal and vertical polarization plane components of  $2^{17}$ -Sph- $D_4$ <sup>2</sup>.

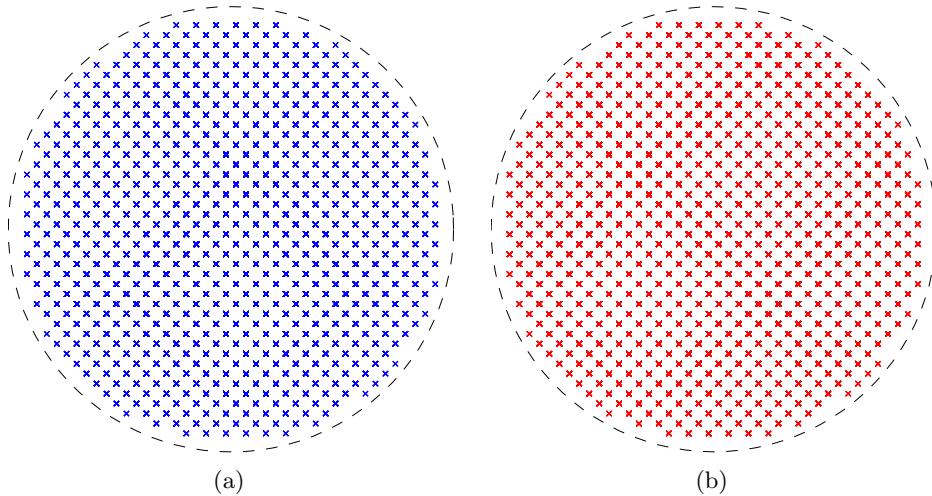


Figure 4.6: Projection of  $2^{17}$ -Sph- $D_4$  constellation on (a) horizontal and (b) vertical polarization planes.

Though  $M$ -Sph- $D_4$  constellation for asymptotically high  $M$  is the best possible con-

<sup>1</sup>Sph has been used in place of spherical to keep the notation compact.

<sup>2</sup>The number preceding the constellation indicates the number of points in the constellation. The power of 2 indicates the number of bits/symbol for the constellation, making it easy for the reader to get an insight into SE directly.

### 4.3. CONSTRUCTION OF 4-D CONSTELLATIONS HAVING $D_4$ LATTICE STRUCTURE

stellation known so far in terms of power efficiency, it is complicated to implement it in practice due to increased detector complexity [30].

#### 4.3.2 Set Partitioning of a 4-D Cubic Constellation

Another modulation format having the  $D_4$  lattice structure can be obtained starting from a four-dimensional cubic constellation. Such structures were proposed in [12, 30] and referred to as SP-QAM (Set Partitioned QAM). They can be easily constructed from a  $2^{4m}$  point cubic  $Z_4$  integer lattice by retaining only those points whose coordinates add to an even sum (set partitioning). The constellation obtained has  $2^{4m-1}$  points with  $D_4$  lattice structure. The SP-QAM constellation is bounded by a cubical boundary rather than a spherical boundary, as a result it has slightly lower power efficiency compared to Sph- $D_4$ .

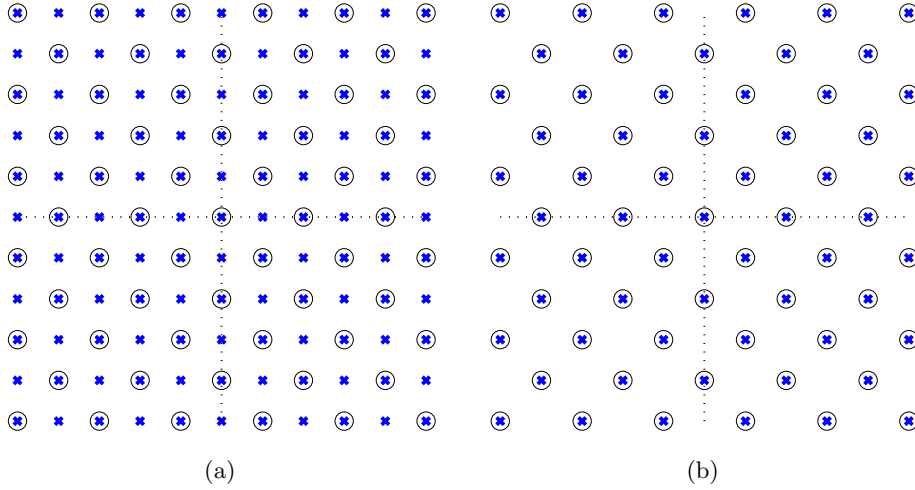


Figure 4.7: 2-D analogy of set partitioning for construction of  $D_4$  constellations from cubic constellation. (a) Cubic constellation and (b) constellation obtained by set partitioning.

Figures 4.7(a) and 4.7(b) give a 2-D analogy of set partitioning.  $Z_2$  in Figure 4.7(a) is the cubic lattice structure similar to rectangular QAM and Figure 4.7(b) shows the constellation formed by set partitioning of  $Z_2$ .

#### 4.3.3 Union of Two 4-D Cubical Constellation

The other modulation format having  $D_4$  structure is based on the definition of  $D_4^*$ .  $D_4^*$  has the same structure as  $D_4$  but different orientation [29]. According to the definition,

$$D_4^* = Z_4 \cup \left( \left[ \begin{array}{c} 1 \\ 2 \end{array} \right]_4 + Z_4 \right), \quad (4.4)$$

### 4.3. CONSTRUCTION OF 4-D CONSTELLATIONS HAVING $D_4$ LATTICE STRUCTURE

---

where  $Z_4$  is the integer cubic lattice (structure of DP-QAM constellations) and  $[\frac{1}{2}]_4 = [\frac{1}{2}, \frac{1}{2}, \frac{1}{2}, \frac{1}{2}]$ . Figure 4.8 shows the 2-D analogy of the construction method. This construction method is similar to the method described in Section 4.2.1. The centroid of the constructed constellation is calculated and moved to zero to minimize the average symbol energy. Since this construction also has  $D_4$  lattice arrangement, the constellation generated is referred to as SP-QAM [30]. The union of two  $2^{4m}$ -DP-QAM results in  $2^{4m+1}$ -SP-QAM.

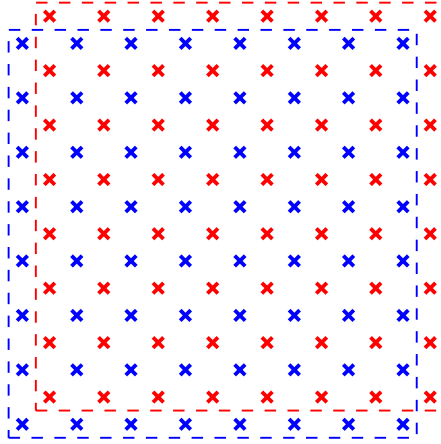


Figure 4.8: 2-D analogy of construction of  $D_4$  constellations using a cubic constellation and its shifted version.

Though the last two constructions described do not have spherical boundaries, they are relatively easy to construct and most importantly very efficient detection methods exist for such structures [29]. In Chapter 5 two detection algorithms will be described for these constellations.

Though both constellations constructed in sections 4.3.2 and 4.3.3 have  $D_4$  lattice structure, they differ in their outer boundaries as evident from Figures 4.7(b) and 4.8. To distinguish them when necessary, SP-QAM A and SP-QAM B will be used to refer to the constellation constructed in Section 4.3.2 and 4.3.3, respectively. That is,

- SP-QAM A:** Set Partitioned QAM constructed from set partitioning method,
- SP-QAM B:** Set Partitioned QAM constructed from union of two cubic constellations.

## Summary

This chapter pointed out the possibility of improving the spectral efficiency of dual polarization communication systems by considering modulation in four-dimensional signal space. The reasons for DP-QAM constellations being suboptimal in terms of power efficiency was highlighted and more efficient modulation formats were introduced. Finally, the construction of three different modulation formats having  $D_4$  structure was



### 4.3. CONSTRUCTION OF 4-D CONSTELLATIONS HAVING $D_4$ LATTICE STRUCTURE

---

discussed.

## Chapter 5

# Performance and Detection of 4-D Modulations

Chapter 4 introduced spectrally efficient modulations in four dimensions and discussed their construction techniques in detail. In this chapter performance measures of modulation formats as stated in Chapter 3 are discussed for  $D_4$  and compared with other formats.

### 5.1 Asymptotic Power Efficiency and Spectral Efficiency

The expression for asymptotic power efficiency is given in Eqn. 3.5. To compute the asymptotic power efficiencies of different constellation, the constellations are generated such that the  $d_{\min}$  is constant and then the average symbol energy  $E_s$  is determined. Table 5.1 lists the PE and SE of the various possible four-dimensional modulation formats. The notation **Sph** is used to represent constellations with spherical boundaries.

To compare the modulations directly from the numerical values of the PE, they should have the same number of levels  $M$ . It is not possible to construct SP-QAM constellation with same number of levels as in DP-QAM, which makes direct and fair comparison difficult. However, Sph- $D_4$  and Sph-DP-QAM both having spherical boundaries and same number of levels can be compared. Table 5.2 shows such comparison.

Table 5.2 highlights the possible use of constellations extracted from  $D_4$  lattice as *power efficient* modulations. For the same spectral efficiency Sph- $D_4$  has higher asymptotic power efficiency than Sph-DP-QAM. The power efficiency of  $D_4$  constellation over cubic constellation has been discussed in depth in [1] as a power efficient modulation for coherent optical communication system. The constellation with eight points having  $D_4$  lattice structure referred to as Polarization Switched QPSK (PS-QPSK) is shown to have PE of 1.76 dB over BPSK constellation [1].

The previous chapter described the spectral efficient side of  $D_4$  constellations in comparison to cubic constellations in 4-D. From Table 5.2, the  $D_4$  constellations can also be viewed as power efficient. This implies that the  $D_4$  constellations can be viewed as

Table 5.1: Comparison between selected DP-QAM and  $D_4$  constellations

Format	Lattice structure	Boundary	No.of levels $M$	$2 \times \text{SE}$	PE[dB]
DP-QPSK	Cubic	Cubic	16	4	0
256-DP-QAM	Cubic	Cubic	256	8	-3.98
256-Sph-DP-QAM	Cubic	Spherical	256	8	-3.77
$(64 \times 64)$ -DP-QAM	Cubic	Cubic	4096	12	-8.45
$(64 \times 64)$ -Sph-DP-QAM	Cubic	Spherical	4096	12	-8.07
PS-QPSK	$D_4$	cubic	8	3	1.76
32-SP-QAM	$D_4$	cubic	32	5	0
128-SP-QAM	$D_4$	cubic	128	7	-1.55
256-Sph- $D_4$	$D_4$	Spherical	256	8	-2.31
512-SP-QAM	$D_4$	cubic	512	9	-3.679
$(64 \times 64/2)$ -SP-QAM	$D_4$	cubic	2048	11	-5.818
$(64 \times 64)$ -Sph- $D_4$	$D_4$	Spherical	4096	12	-6.56
$(64 \times 64 \times 2)$ -SP-QAM	$D_4$	cubic	8192	13	-8.15

Table 5.2: Comparison between Sph-DP-QAM and Sph- $D_4$  constellation

No.of levels $M$	Format	PE[dB]	Format	PE[dB]
256	256-Sph-DP-QAM	-3.77	256-Sph- $D_4$	-2.31
$(64 \times 64)$	$(64 \times 64)$ -Sph-DP-QAM	-8.07	$(64 \times 64)$ -Sph- $D_4$	-6.56
$(256 \times 256)$	$(256 \times 256)$ -Sph-DP-QAM	-12.83	$(256 \times 256)$ -Sph- $D_4$	-11.33

either power efficient or spectrally efficient, depending on with which cubic constellation they are being compared with.

A fair method of comparing modulations is to plot the constellations as a point in a plane that relates both spectral efficiency and power efficiency. Such plots are used in [30] to compare constellations. Figure 5.1 shows spectral efficiency (SE) vs. sensitivity penalty ( $1/\text{PE}$ ) plot for DP-QAM and SP-QAM modulation formats. Sensitivity penalty is used since the power needed to achieve a required SER is proportional to sensitivity penalty.

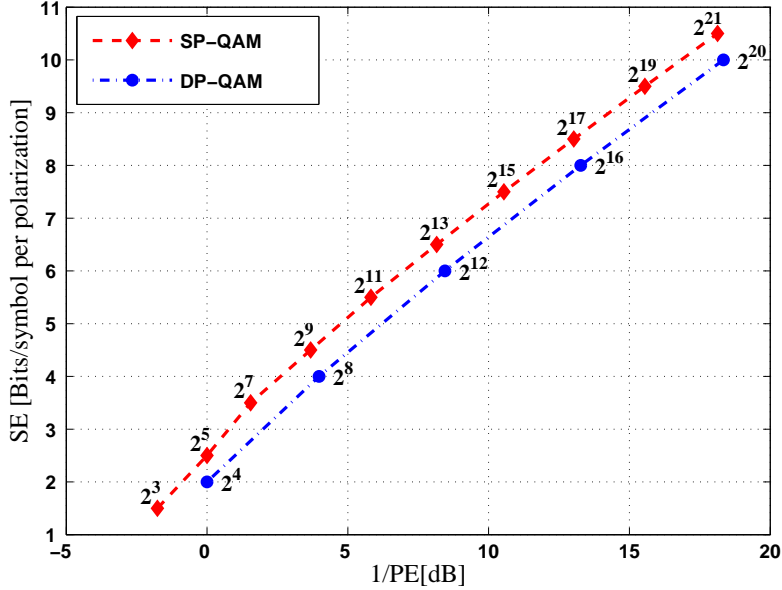


Figure 5.1: Spectral efficiency vs.  $1/PE$  plot for DP-QAM and SP-QAM constellation.

The general performance of the modulation formats can be compared using Figure 5.1. At a fixed spectral efficiency the line corresponding to SP-QAM suggests that SP-QAM format has higher power efficiency than the DP-QAM format. The gain in power efficiency can be considered as *coding gain*<sup>1</sup> which is obtained by changing the structure of the modulation format from cubic to  $D_4$  [24].

Figure 5.2 shows the standard DP-QAM and Sph- $D_4$  constellations on the SE vs.  $1/PE$  plane. The optimal Sph- $D_4$  constellations for lower number of levels have to be found by sphere packing problem simulation. For a reasonable number of levels i.e., for  $SE > 2.2$  [30], the  $M$ -ary spherical subset of  $D_4$  is nearly optimal. The Sph- $D_4$  constellations plotted in the figure are derived by choosing the spherical subsets, which are not optimal for lower spectral efficiencies. At a fixed SE, the Sph- $D_4$  in general are more power efficient than the DP-QAM. The higher power efficiency is due to  $D_4$  structure (coding gain) and spherical boundaries (shaping gain).

<sup>1</sup>Coding gain here refers to the decrease in average symbol energy for the  $D_4$  constellations due to their structure in comparison with DP-QAM constellation having same  $d_{\min}$  and SE.

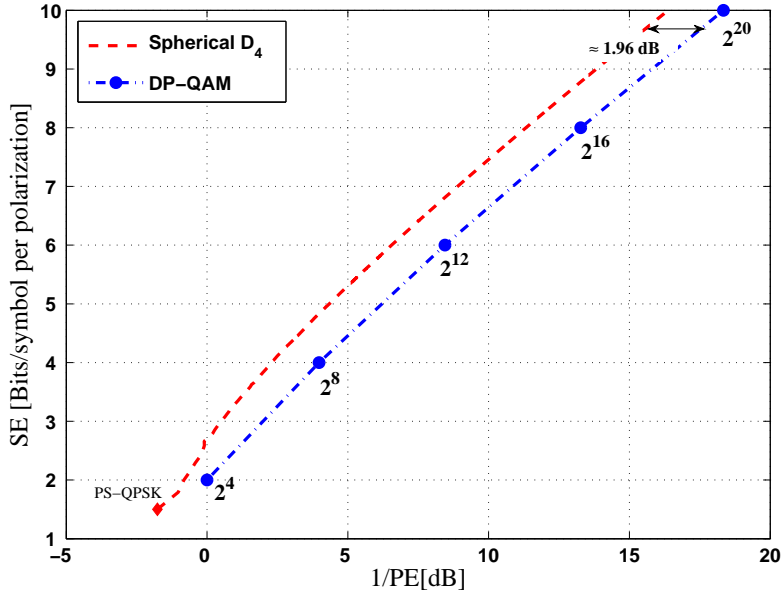


Figure 5.2: Spectral efficiency vs.  $1/PE$  plot for DP-QAM and Sph- $D_4$  constellations.

Figure 5.3 shows  $PE/PE_{\text{PAM}}$  vs. SE plot for 4-D modulations. Such comparison has been made in [30], where  $PE_{\text{PAM}} = \frac{3SE}{2(2^{SE}-1)}$  is the asymptotic power efficiency of one-dimensional pulse amplitude modulation (PAM) with spectral efficiency SE. The figure clearly shows the shaping and coding gains of  $D_4$  constellations with respect to DP-QAM. For higher order constellations the coding gains ( $\gamma_c$ ) and shaping gains ( $\gamma_s$ ) are close to the theoretical values of  $\gamma_c = 1.51$  dB [31, Table 1.2] and  $\gamma_s = 0.46$  dB [24]. The spherical constellations are spherical  $M$ -ary subsets and are near optimal at lower spectral efficiencies. As seen in the figure, SP-QAM A and SP-QAM B follow a different curve to reach the asymptotic shaping and coding gains, this is the direct consequence of their different boundaries. The packing density<sup>2</sup> of  $D_4$  lattice structure is  $\pi^2/16$  [26, Table 1.2]. Since different methods are used to construct SP-QAM A and SP-QAM B, they have different outer boundaries and their packing densities reach  $\pi^2/16$  along different paths as shown in Figure 5.4 .

<sup>2</sup>Packing density in context of the constellations is the ratio of volume of the spheres (replacing the constellation points) to the volume of the smallest cube enclosing them.

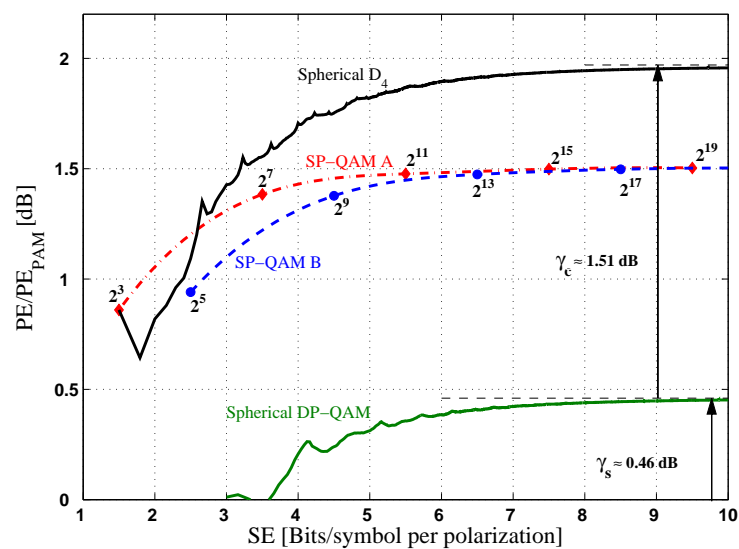


Figure 5.3: PE/PE<sub>PAM</sub> vs. spectral efficiency plot for four-dimensional modulations. The coding gain  $\gamma_c$  and the shaping gain  $\gamma_s$  of the  $D_4$  constellations over the cubic constellation are shown.

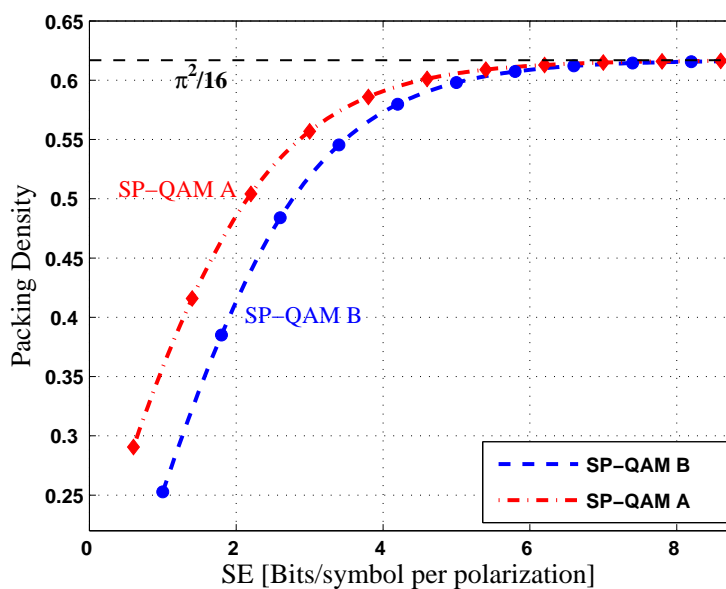


Figure 5.4: Packing density vs. spectral efficiency for SP-QAM modulations.

## 5.2 Non Asymptotic Performance in AWGN Channel

The previous section compared the modulation formats in terms of asymptotic power efficiency and spectral efficiency. It is also necessary to compare the constellations in non asymptotic regions. In this section the constellations are compared in non asymptotic regions.

To get accurate SER vs. SNR curves for higher order constellations (large  $M$ ) through simulations, large number of symbols have to be generated and averaged over several iterations. This requires large computational time and obtaining the curves from simulations is impractical. To solve this theoretical expressions for SER as a function of SNR have to be determined. The theoretical SER curves for DP-QAM constellation can be obtained by just scaling the SER expression of QAM. An exact theoretical SER expression has been derived for PS-QPSK [10]. However, it is difficult to derive exact SER expressions for the other SP-QAM constellations because of their geometry and integration of the 4-D Gaussian noise over the decision regions of the constellation points.

Since deriving exact SER expression is difficult, an upper bound on SER such as union bound is calculated. The bound is calculated using the pair-wise error probability ( $P_{\text{pep}}$ ). When the union bound is approximated by only considering the nearest neighbours i.e., symbols at a distance of  $d_{\text{min}}$ , the error probability obtained is called nearest neighbour approximation. The pair-wise error probability  $P_{\text{pep},d_{\text{min}}}$  for symbols separated by  $d_{\text{min}}$  is given by

$$P_{\text{pep},d_{\text{min}}} = \frac{1}{2} \text{erfc} \left( \frac{d_{\text{min}}}{2\sqrt{N_0}} \right).$$

The above expression is similar to the pair-wise error probability term used in the Eqn. 3.6 for the 2-D constellations, the reason for using the same expression for SP-QAM constellation is described in Appendix A. Using the  $P_{\text{pep},d_{\text{min}}}$  and considering only the nearest neighbours in Eqn. 3.6, the nearest neighbour approximation for SER is given by [17, Eqn. 5.45]

$$\text{SER} \leq \frac{\sum_{k=1}^p N_k V_k}{M} P_{\text{pep},d_{\text{min}}}, \quad (5.1)$$

where  $N_k$  is the number of nearest neighbours the  $k$ th type symbol has,  $V_k$  is the number of times the  $k$ th type symbol repeats in the constellation and  $p$  is the number of different kinds of symbol having different number of nearest neighbours;  $M$  is the total number of symbols in the constellation.

Figures 5.5 and 5.6 show the nearest neighbour approximation SER vs.  $E_b/N_0$  curves for SP-QAM modulation formats. The number of different kinds of symbols, nearest neighbours and the number of times such symbols repeat were counted from the generated constellation through simulation. Tables 5.3 and 5.4 show these values for the considered SP-QAM A and SP-QAM B constellations respectively.

Table 5.3: Nearest neighbour multiplicity table for SP-QAM A constellations

$k$		1	2	3	4	5
$M = 2^3$	$N_k$	6	-	-	-	-
	$V_k$	8	-	-	-	-
$M = 2^7$	$N_k$	6	9	13	18	24
	$V_k$	8	32	48	32	8
$M = 2^{11}$	$N_k$	6	9	13	18	24
	$V_k$	8	96	432	864	648
$M = 2^{15}$	$N_k$	6	9	13	18	24
	$V_k$	8	224	2352	10976	19208
$M = 2^{19}$	$N_k$	6	9	13	18	24
	$V_k$	8	480	10800	108000	405000

Table 5.4: Nearest neighbour multiplicity table for SP-QAM B constellations

$k$		1	2	3	4	5	6	7	8	9	10	11	12	13	14	15
$M = 2^5$	$N_k$	5	6	8	12	20	-	-	-	-	-	-	-	-	-	-
	$V_k$	2	8	12	8	2	-	-	-	-	-	-	-	-	-	-
$M = 2^9$	$N_k$	5	6	7	8	9	10	12	13	14	15	20	21	22	23	24
	$V_k$	2	8	16	12	48	48	8	48	96	64	2	16	48	64	32
$M = 2^{13}$	$N_k$	5	6	7	8	9	10	12	13	14	15	20	21	22	23	24
	$V_k$	2	8	48	12	144	432	8	144	864	1728	2	48	432	1728	2592
$M = 2^{17}$	$N_k$	5	6	7	8	9	10	12	13	14	15	20	21	22	23	24
	$V_k$	2	8	112	12	336	2352	8	336	4704	21952	2	112	2352	21952	76832
$M = 2^{21}$	$N_k$	5	6	7	8	9	10	12	13	14	15	20	21	22	23	24
	$V_k$	2	8	240	12	720	10800	8	720	21600	216000	2	240	10800	216000	1620000

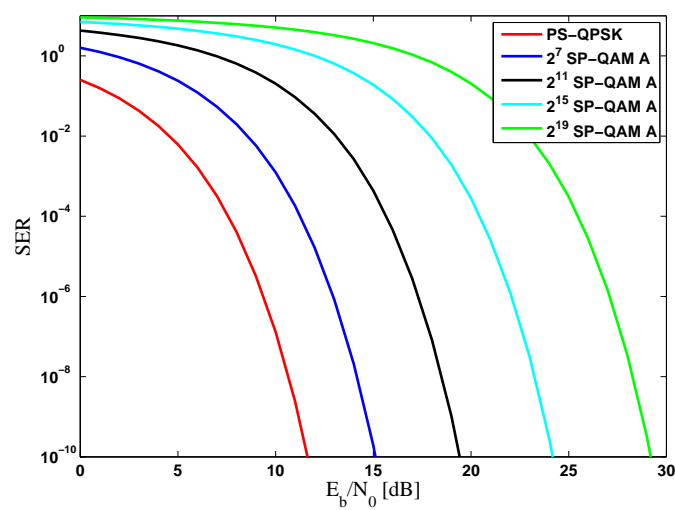


Figure 5.5: The nearest neighbour approximation SER curves of SP-QAM A modulation formats.



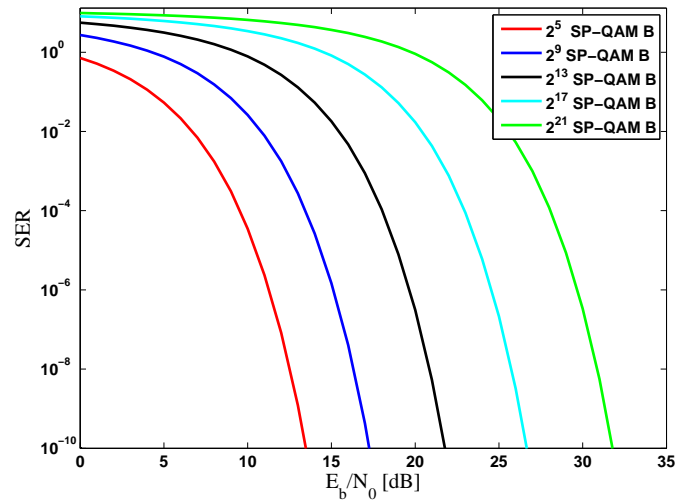


Figure 5.6: The nearest neighbour approximation SER curves of SP-QAM B modulation formats.

The tightness of the bound is verified using SER simulations for the lower order SP-QAM. Figure 5.7 shows the simulated SER curves along with the nearest neighbour approximation SER for lower order SP-QAM constellations. As seen in Figure 5.7 the SER approximation is close to the simulated curve at higher SNRs. High SNR being relative to the number of levels in the modulation format, the SNRs corresponding to SER lower than  $10^{-4}$  can be considered as high SNRs.

The SER approximation being close to the exact SER curves for SERs nearly equal to  $10^{-3}$  and lower, receiver sensitivity for SP-QAM constellations can be obtained from the theoretical SER approximation derived. Following which, spectral efficiency vs. receiver sensitivity plot can be drawn for SP-QAM constellations.

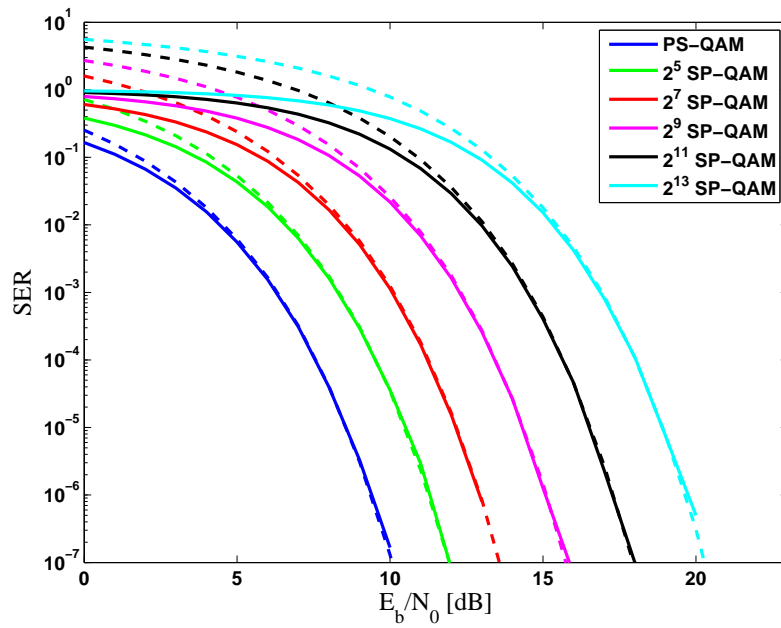


Figure 5.7: SER vs. SNR curves for the selected SP-QAM constellations. The solid curves are obtained from the simulations and the dashed curves are plotted using the nearest neighbour approximation SER expression derived. SER approximation curves follow the exact SER curves from SERs of nearly  $10^{-3}$  and lower.

## Spectral Efficiency vs. Receiver Sensitivity

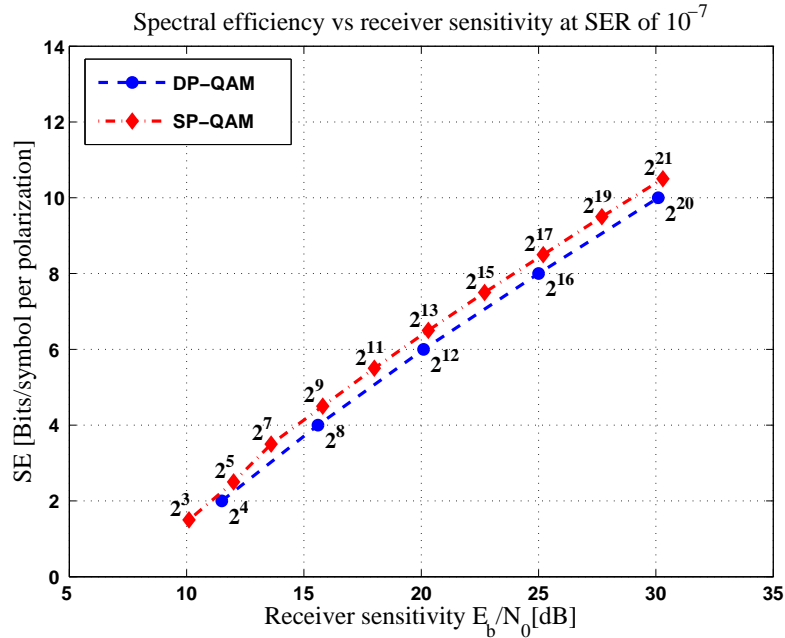


Figure 5.8: Spectral efficiency vs. receiver sensitivity at  $\text{SER} = 10^{-7}$  for SP-QAM and DP-QAM constellations along with Shannon limit.

Figure 5.8 shows the spectral efficiency vs. receiver sensitivity plot at a fixed SER of  $10^{-7}$  for DP-QAM and SP-QAM constellations in AWGN channel. Comparing the constellations at a fixed SER of  $10^{-7}$  is a reasonable choice when these formats are to be used in LoS microwave links where SNRs on an average are high. The numbers in front of the markers indicate the number of constellation points. At a fixed spectral efficiency the SP-QAM curve has better receiver sensitivity, reflecting the higher power efficiency of the SP-QAM constellations.

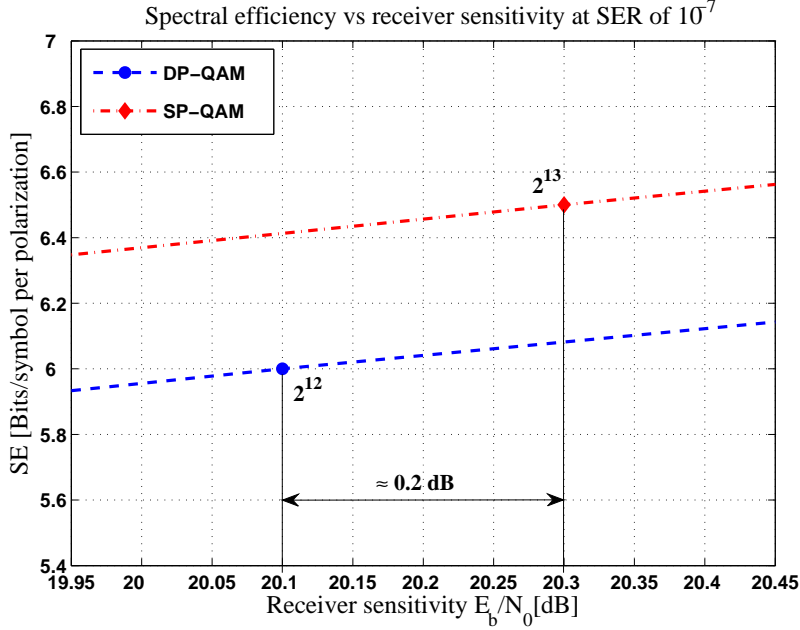


Figure 5.9: Spectral efficiency vs. receiver sensitivity for  $2^{13}$ -SP-QAM and  $2^{12}$ -DP-QAM at  $\text{SER} = 10^{-7}$ .

To get an insight into SE, consider  $2^{13}$ -SP-QAM and  $2^{12}$ -DP-QAM as shown in Figure 5.9. The constellation  $2^{13}$ -SP-QAM has a SE 0.5 bits/symbol per polarization higher than the SE of  $2^{12}$ -DP-QAM and this gain is at a cost of very small increase in the receiver sensitivity. The additional receiver sensitivity is approximately  $E_b/N_0 = 0.2$  dB at  $\text{SER}=10^{-7}$ . This result shows that, at an expense of very small increase in energy per bit, an increase in spectral efficiency can be achieved by making use of SP-QAM constellation in place of DP-QAM.

The difference in the receiver sensitivity for the pairs ( $2^8$ -DP-QAM and  $2^9$ -SP-QAM), ( $2^{12}$ -DP-QAM and  $2^{13}$ -SP-QAM), ( $2^{16}$ -DP-QAM and  $2^{17}$ -SP-QAM), ( $2^{20}$ -DP-QAM and  $2^{21}$ -SP-QAM) reduces as the SER is decreased. At very low SERs, the receiver sensitivity of the SP-QAMs drops below their DP-QAM counterparts in the above mentioned pairs, this is because at higher SNRs the contribution of neighbouring points to the SER decreases. Figure 5.10 shows the SE vs. receiver sensitivity plot for middle order constellations at  $\text{SER}=10^{-20}$ . The  $2^9$ -SP-QAM and  $2^{13}$ -SP-QAM have lower receiver sensitivities than  $2^8$ -DP-QAM and  $2^{12}$ -DP-QAM, respectively. This result is in agreement with the fact that the SP-QAM constellations have higher asymptotic power efficiencies than their counterparts as shown in Table 5.1.

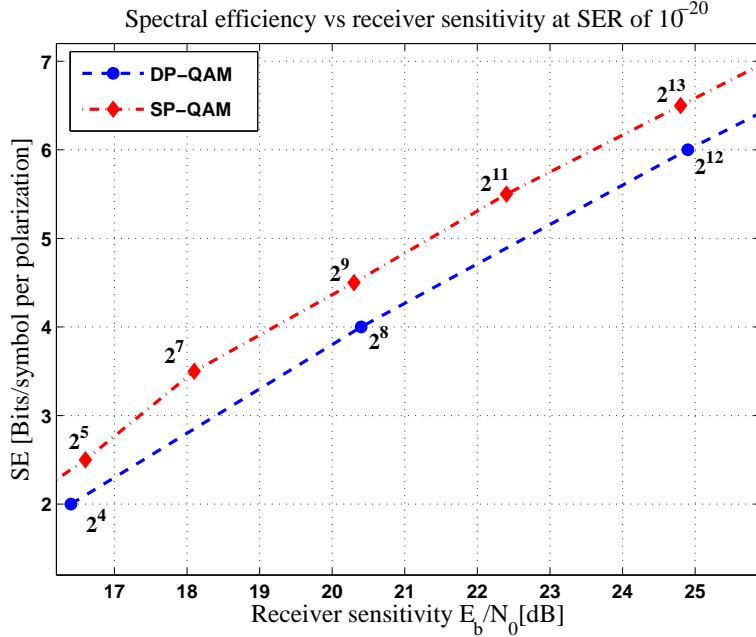


Figure 5.10: Spectral efficiency vs. receiver sensitivity for middle order SP-QAM and DP-QAM constellations at  $\text{SER} = 10^{-20}$ .

From Figure 5.10 it is seen that the receiver sensitivity of  $2^5$ -SP-QAM is still higher than that of  $2^4$ -DP-QAM. This is because although  $2^5$ -SP-QAM has  $D_4$  structure, its packing density is far from the packing density of  $D_4$  lattice structure due to its method of construction and fewer number of points.

### Comment on Increased Spectral Efficiency

The transition from non-polarized single carrier communication to dual polarization multiplexing and making use of  $M$ -QAM in each polarization resulted in doubling of SE. Compared to that improvement, the gain obtained using the SP-QAM modulation format looks insignificant. When  $2^8$ -DP-QAM and  $2^9$ -SP-QAM are compared, the increase in SE is approximately 10%, for  $2^{20}$ -DP-QAM and  $2^{21}$ -SP-QAM the increase is 5%. Though, increasing the order of SP-QAM constellation reduces the percentage increase in SE, the increase in the net bit rate is significant given the high bit rates supported by LoS microwave links using DP-QAM.

For example, at MWC 2011 (Mobile World Congress) Ericsson demonstrated a record spectral efficiency of 32.1 bps/Hz using 512 QAM in 4x4 LoS MIMO with polarization multiplexing [19]. By using  $2^{19}$ -SP-QAM in place of two separate 512-QAMs in the horizontal and vertical polarization pair, the spectral efficiency can be increased by nearly 5% resulting in SE of 33.7 bps/Hz. This improvement is at an expense of small increase in energy requirement.

### 5.3 Constrained Capacity Curves

The capacity of a memoryless channel with input signal space  $X$  and output signal space  $Y$  is equal to the result of the maximization of the mutual information over all possible input distributions  $p_X(x)$  [32], i.e.,

$$C = \max_{p_X} \{I(X; Y)\},$$

where  $I(X; Y)$  is the average mutual information between the random variables  $X$  and  $Y$  and is given by

$$I(X; Y) = \int \int_{\mathcal{X}, \mathcal{Y}} p_{X,Y}(x,y) \log_2 \frac{p_{X,Y}(x,y)}{p_X(x)p_Y(y)} dx dy. \quad (5.2)$$

The capacity of a channel can be interpreted as the maximum information rate allowing a reliable transmission [32]. When the  $p_X(x)$  is fixed i.e., for a specific distribution or a fixed constellation, the capacity is called *constellation constrained capacity* or *constrained capacity*. It gives the upper bound to the achievable information rates on the channel for the given constellation. For the discrete uniform  $M$ -ary modulations, the following expression has been derived in [33].

$$I(X; Y) = \log_2(M) - \frac{1}{M} \sum_{\mathcal{X}} \int_{\mathcal{Y}} p_{Y|X}(y|x) \log_2 \left( \frac{\sum_{x' \in \mathcal{X}} p_{Y|X}(y|x')}{p_{Y|X}(y|x)} \right) dy. \quad (5.3)$$

In this section the constrained capacity curves as a function of SNR are plotted for a few selected SP-QAM and DP-QAM constellations.

#### 5.3.1 Constrained Capacity in AWGN Channel

Consider the transmission of symbol  $X$  over the AWGN channel, the output at the end of the matched filter  $Y$  is given by

$$Y = X + W,$$

where  $W \sim \mathcal{N}(0, 2\sigma^2)$  is two-dimensional complex Gaussian noise with zero mean and variance  $2\sigma^2$  for two-dimensional modulations and its probability distribution function is given by  $p_W(w) = \frac{1}{2\pi\sigma^2} \exp \frac{-|w|^2}{2\sigma^2}$ , where  $\frac{1}{2\sigma^2}$  is the SNR when the input average power is normalized to 1. As a result the probability distribution function of the received symbols given the transmitted symbol becomes  $p_{Y|X}(y|x) = p_W(y - x)$ . Substituting this in Eqn. 5.3 we obtain,

$$I(X; Y) = \log_2(M) - \frac{1}{M} \sum_{\mathcal{X}} \int_{\mathbb{R}^2} p_W(y - x) \log_2 \left( \frac{\sum_{x' \in \mathcal{X}} p_W(y - x')}{p_W(y - x)} \right) dy. \quad (5.4)$$

Solving the expression further (as in [33]) and replacing the integration by expectation over the noise variable we obtain the following expression which allows the computation of mutual information by Monte Carlo method.

$$I(X;Y) = \log_2(M) - \frac{1}{M} \sum_{x \in \mathcal{X}} \mathbb{E}_W \left[ \log_2 \left( \sum_{x' \in \mathcal{X}} \exp \frac{|W|^2 - |W + x - x'|^2}{2\sigma^2} \right) \right]. \quad (5.5)$$

In the above expression the integral term over  $\mathbb{R}^2$  has been replaced by the expectation, as a result the expression holds good for modulation formats of higher dimension. Using the above expression the constrained capacity curves for the DP-QAM and SP-QAM constellation is plotted. Figure 5.11 shows the constrained capacity curves of SP-QAM and DP-QAM constellations in AWGN channel.

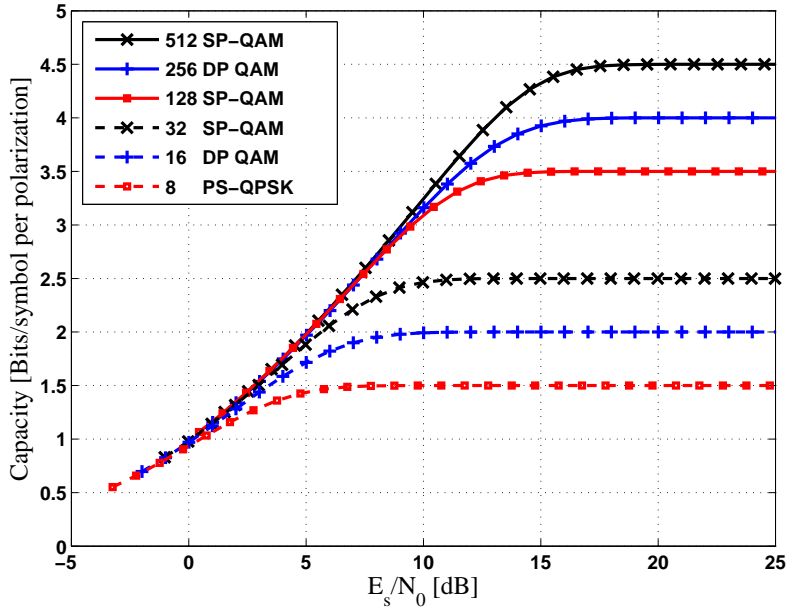


Figure 5.11: Constrained capacity curves for DP-QAM and SP-QAM constellations in AWGN channel.

### 5.3.2 Constrained Capacity in Partially Coherent AWGN Channel

The expression for constrained capacity in PC-AWGN channel with Tikhonov distributed phase noise has been derived in Appendix B.

Figure 5.12 shows the constrained capacity curves of a few lower order 4-D constellations, the parameter  $\rho$  for the Tikhonov distribution has been set to 50 in these curves. The figure also shows the constrained capacity curves of the constellations in AWGN and it can be observed that additional SNR is required to reach a given capacity in PC-AWGN in comparison to AWGN.

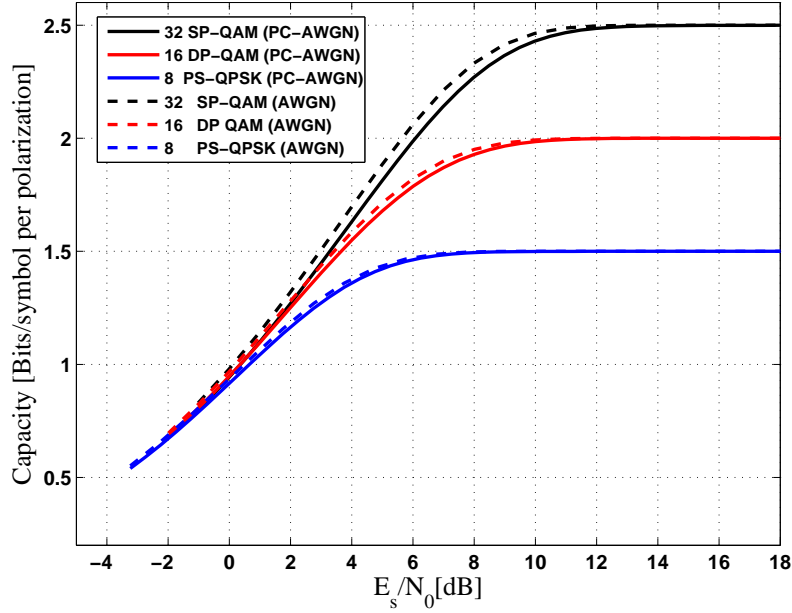


Figure 5.12: Constrained capacity curves for DP-QAM and SP-QAM constellations in partially coherent-AWGN channel with Tikhonov-distributed phase noise having  $\rho = 50$ .

## 5.4 Detector Complexity

The communication systems with high symbol rates put a constraint on the modulation formats to have low detection complexities. The detection of received symbols should be made in a reasonable time duration to prevent delay. Detection complexity with respect to time required in detecting a constellation point is a function of many parameters such as the algorithm used, hardware implementation and the resolution of analog to digital conversion. In this section, detector complexity is discussed in context of algorithm only.

### 5.4.1 Detection of 2-D Constellations

The DP-QAM or two separate QAMs used in the dual polarized systems have a cubical geometry and the detection complexity of the cubic QAM constellations is low. Figure 5.13 shows the 16-QAM constellation. When the channel considered is AWGN, the Voronoi regions of the constellation determine the detection boundaries. The Voronoi region of each symbol has unique set of projections on the In-phase and Quadrature axes. Figure 5.13 shows the projection of the Voronoi region of constellation point  $c_{13}$ . Owing to the non overlapping nature of the projections of Voronoi regions, the detection of received symbols is simple. By taking the projection of received symbol on both axes, it is possible to detect the received symbol.

If the projections of Voronoi regions of the constellation points overlap, then the



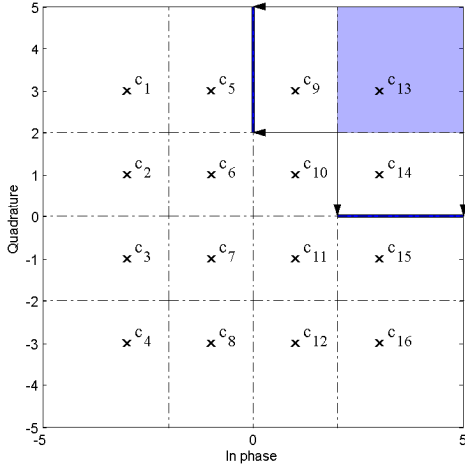


Figure 5.13: 16-QAM constellation with Voronoi regions of the constellation points.

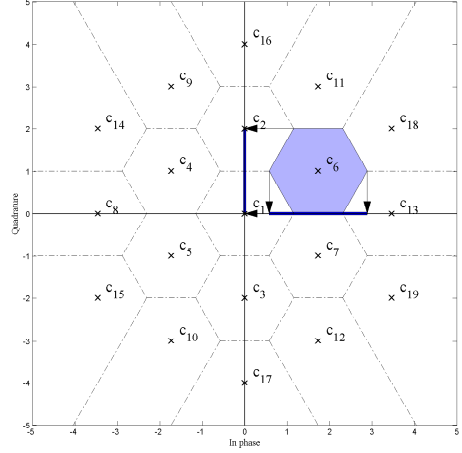


Figure 5.14: 2-D hexagonal constellation with Voronoi regions of the constellation points.

detection is not straight forward. Figure 5.14 shows a hexagonal constellation with the Voronoi regions of the constellation points. In Figure 5.14 the projection of Voronoi region of the constellation point  $c_6$  is shown. If the projections of the Voronoi regions of the neighbouring constellation points are drawn, they overlap with this projection; hence, detection by just projection is not possible. The most obvious way to detect the symbols is using exhaustive search method, which is computationally demanding. Though the detection at first glance looks complex, the complexity of detection can be reduced by taking into consideration the regular geometry of the constellation.

The spectrally efficient SP-QAM modulation formats and their performance was discussed in the previous sections. For those modulation formats to be practically feasible in high data rate communication systems, their detection complexity has to be studied. Section 4.3 describes the construction of SP-QAM constellation from DP-QAM cubic constellation which suggests that the SP-QAM constellation has  $D_4$  structure and is not cubic in geometry. As a result the direct projection of symbols onto orthogonal axes is not enough to detect the symbols. The following section describes two low complexity detectors for SP-QAM format.

### 5.4.2 Detector for $D_4$ Constellations Based on Set Partitioning Principle

This method of detection is based on the construction of SP-QAM from the set partitioning of cubic lattices described in Section 4.3.2. The detection method was proposed in [29]. Consider the sampled received symbol  $r = c + w$ . To detect the received symbol, the cubic constellation  $2^{4m}$ -DP-QAM from which  $2^{4m-1}$ -SP-QAM **A1** is constructed is considered (as described in Figure 5.15). The constellation point  $c'_1$  in DP-QAM which is

closest to  $r$  and the constellation point  $c'_2$  in DP-QAM which is next closest to  $r$  are determined. The points  $c'_1$  and  $c'_2$  will be adjacent points on DP-QAM. Since SP-QAM **A1** is formed by the set partitioning of DP-QAM, only one among  $c'_1$ ,  $c'_2$  belongs to SP-QAM **A1**. The constellation point belonging to SP-QAM **A1** is the detected symbol.

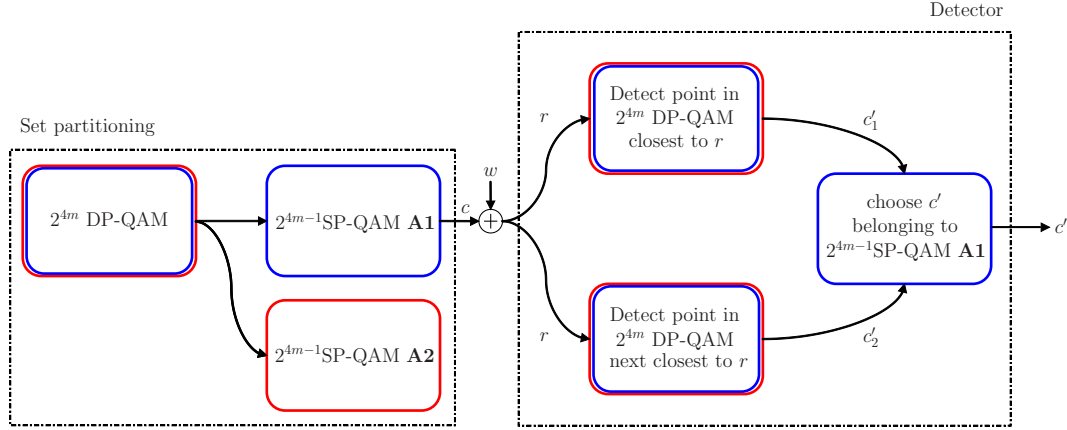


Figure 5.15: Schematic diagram showing the low complexity detector algorithm based on set partitioning.

Figure 5.15 summarizes the principle behind the method. Detailed algorithm for the method can be found in [29, sec 3,4].

### 5.4.3 Alternate Detector for $D_4$ constellation

This method also relies on the geometry of the SP-QAM constellations and the construction method. This method is based on construction of SP-QAMs by the union of two DP-QAMs as described in Section 4.3.3. The construction procedure is given by

$$2^{4m+1}\text{-SP-QAM} = 2^{4m}\text{-DP-QAM} \cup \left( \left[ \frac{d_{\min}}{2} \right]_4 + 2^{4m}\text{-DP-QAM} \right), \quad (5.6)$$

for simplicity it can be expressed as

$$\text{SP} = \text{DP}_1 \cup \text{DP}_2.$$

Consider constellation point  $c$  chosen from SP for transmission. The sampled received symbol is  $r = c + w$ , where  $w$  is the noise. From the above description, the constellation point  $c$  chosen from SP constellation for transmission belongs to either  $\text{DP}_1$  or  $\text{DP}_2$ . This property leads to a simple detector algorithm. The received symbol  $r$  is detected with respect to  $\text{DP}_1$  and  $\text{DP}_2$  separately to result in two possible output constellation points  $c'_1$  and  $c'_2$ , respectively. Owing to the cubic nature of  $\text{DP}_1$  or  $\text{DP}_2$ , the detection complexity is low as explained for 16-QAM earlier. Now the received symbol  $r$  has two possible constellation points as transmitted point. Among  $c'_1$  and  $c'_2$  the one closer to

$r$  is determined and referred as  $c'$ , which is the detected constellation point. The block diagram in Figure 5.16 gives the top level description of the detector algorithm.

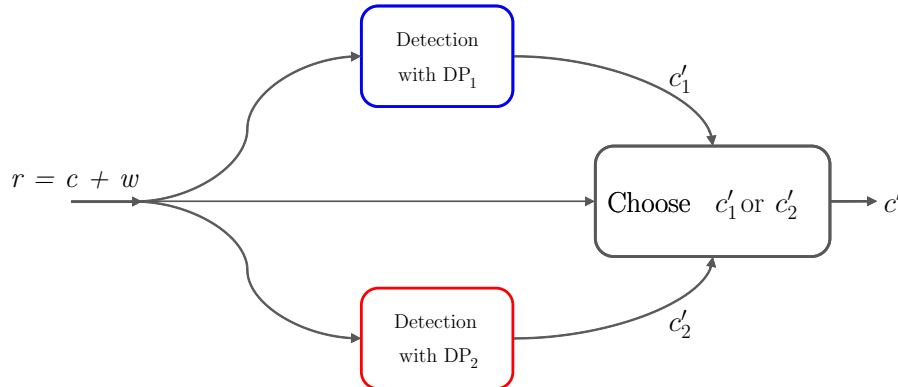


Figure 5.16: Schematic diagram of low complexity detector for SP-QAM modulation formats.

The advantage of this algorithm is that it uses the detector algorithm for cubic constellations. Since the cubic modulation formats have been in use for a long time, there exist very efficient algorithms and implementations as described in Section 5.4.1. The complete detection algorithm for SP-QAM uses two such implementations and an extra step to chose between  $c'_1$  and  $c'_2$ . The complexity of an algorithm is specified by the number of real additions and multiplications it requires. Complexity of the two detection methods can be compared by computing the number of computations each of them require.

Both detection algorithms were compared to the exhaustive search detector in simulations and both algorithms give the same results as the exhaustive search detector. Hence, the discussed algorithms perform maximum likelihood detection.

## 5.5 Synchronization

In dual polarized systems and spatially separated systems where the streams on different polarization or spatially separated streams are treated as separate streams, the received symbols at each stream are detected separately. As a consequence the delay between the reception of symbols on different streams does not affect the detection. Where as in joint modulation schemes, the delay between the receptions of symbols on different streams has a huge impact on the detection. This section addresses the problem of synchronization in joint modulation schemes.

Let us consider the XPIC system as an example of a system having two independent streams. In case of XPIC the independent streams are the result of polarization multiplexing. The Eqn. 5.7 shows the queue of the symbols on the transmitter side.

$$\begin{bmatrix} I_H(n) & I_H(n-1) & \cdots & I_H(1) & I_H(0) \\ Q_H(n) & Q_H(n-1) & \cdots & Q_H(1) & Q_H(0) \\ I_V(n) & I_V(n-1) & \cdots & I_V(1) & I_V(0) \\ Q_V(n) & Q_V(n-1) & \cdots & Q_V(1) & Q_V(0) \end{bmatrix} \quad (5.7)$$

If the channel introduces unequal delays in each stream the order of the symbols can be altered as shown in Eqn. 5.8. Since the  $I$  and  $Q$  components are modulated by the same carrier on each stream, they are not subjected to relative delay. If the horizontal and vertical polarizations are treated separately the relative shift of the symbol order does not have any effect on the detection as the symbols will be detected independently. But if joint modulation formats are used, the symbols from both polarizations are input to the detector together. The detector thus jointly processes  $[I'_H(n) Q'_H(n) I'_V(n+\tau) Q'_V(n+\tau)]$  instead of  $[I'_H(n) Q'_H(n) I'_V(n) Q'_V(n)]$ , where  $\tau$  is the relative delay. The joint detection leads to error in detection.

$$\begin{bmatrix} I'_H(n) & I'_H(n-1) & \cdots & I'_H(1) & I'_H(0) \\ Q'_H(n) & Q'_H(n-1) & \cdots & Q'_H(1) & Q'_H(0) \\ I'_V(n+\tau) & I'_V(n-1+\tau) & \cdots & I'_V(1+\tau) & I'_V(\tau) \\ Q'_V(n+\tau) & Q'_V(n-1+\tau) & \cdots & Q'_V(1+\tau) & Q'_V(\tau) \end{bmatrix} \quad (5.8)$$

To overcome the problem, some synchronization strategies have to be incorporated. One simple method is to include frame alignment words (FAW) at constant intervals at the transmitter and use this knowledge at receiver to align the symbols on independent streams (e.g., horizontal and vertical polarization streams). Eqn. 5.9 shows the queue of the symbols to be transmitted. FAW is a known sequence of symbols inserted after every  $k$  symbols. The FAW on the independent streams can be used at the receiver to align the streams.

$$\begin{bmatrix} \cdots & I_H(k) & \text{FAW}_H & I_H(k-1) & \cdots & I_H(1) & I_H(0) & \text{FAW}_H \\ \cdots & Q_H(k) & \text{FAW}_H & Q_H(k-1) & \cdots & Q_H(1) & Q_H(0) & \text{FAW}_H \\ \cdots & I_V(k) & \text{FAW}_V & I_V(k-1) & \cdots & I_V(1) & I_V(0) & \text{FAW}_V \\ \cdots & Q_V(k) & \text{FAW}_V & Q_V(k-1) & \cdots & Q_V(1) & Q_V(0) & \text{FAW}_V \end{bmatrix} \quad (5.9)$$

Figure 5.17 is a top level view of synchronization using FAW. The symbols received on both streams are passed through a frame alignment block. In the frame alignment block the symbols are correlated with the respective FAWs to compute the delay in each stream. The individual delays or their difference is output as offsets. The offsets are then fed to a buffer preceding the detector, where the symbols from both streams are aligned using the offsets.

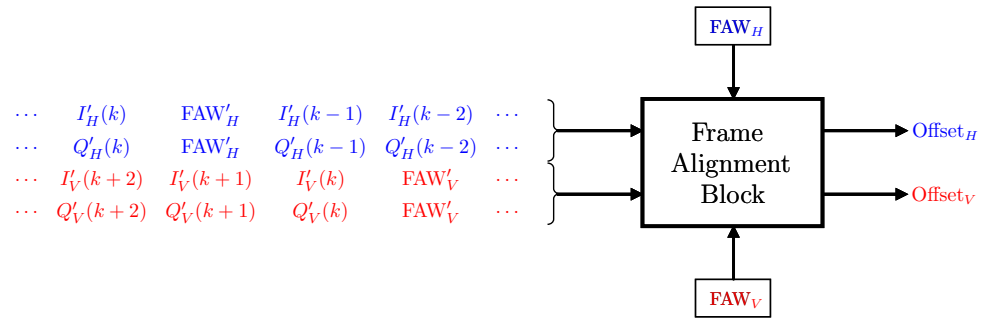


Figure 5.17: Schematic view of synchronization using frame alignment word. The diagram shows the misalignment of the received symbols and how they can be aligned by correlating with FAW.

## Summary

The performance of SP-QAM and spherical- $D_4$  constellations introduced in Chapter 4 were discussed and compared to the DP-QAM constellations. The approximate theoretical SER expression was derived and capacity curves for a few selected constellations were plotted. Finally, two low complexity detectors for SP-QAM constellations were explained.

## Chapter 6

# Eight-Dimensional Joint Modulation Formats

In Chapter 5 the performance of four-dimensional joint modulation formats was analysed. It is seen that spectral and power efficient modulations in 4-D can be constructed by using  $D_4$  lattice structures. PS-QPSK is an example of power efficient modulation format that offers an asymptotic power gain of 1.76 dB over BPSK (baseline), the best known gain known so far [10].

It has been explained in Chapter 4 that dual polarized systems can be viewed as having four dimensional signal space giving 4 DOF. The degree of freedom can be further increased by additionally using space or time multiplexing. One such example is SS-DP-LoS MIMO explained in Section 2.3.4 that uses both space and polarization multiplexing resulting in eight parallel independent streams. These eight independent channels can be processed jointly to produce eight-dimensional signal space. Since increasing the number of dimensions of signal space increases DOF, by optimal use of the higher DOF, power and spectral efficient modulation formats can be constructed.

In this chapter the performance of different 8-D joint modulation formats are analysed.

### 6.1 Eight Dimensional Packing Structures

As stated in Chapter 3, the problem of finding the most power efficient modulation for AWGN channel in an  $N$ -dimensional space is equivalent to finding the densest packing structure of  $N$ -spheres. In this section three possible packing arrangements for 8-D constellation are discussed.

#### 6.1.1 $Z_8$ -QAM

$Z_8$ -QAM follows eight-dimensional  $Z_8$  cubic integer lattice structure.  $Z_8$ -QAM can be interpreted as having eight parallel streams and independent identical ASK on each of

them. Since  $Z_8$ -QAM follows the cubic structure, its performance is similar to the standard 2-D QAM just like DP-QAM. The projection of  $M$ - $Z_8$ -QAM on any 2 orthogonal components looks exactly like  $(\sqrt[8]{M})^2$ -QAM.

### 6.1.2 $D_8$ -QAM

$D_8$ -QAM constellation has the structure of  $D_8$  lattice. The  $D_8$  structure follows the similar construction procedure as the construction of  $D_4$  from  $Z_4$  as described in Section 4.3.  $D_8$  lattice contains those points on eight-dimensional integer lattice  $Z_8$ , whose co-ordinates sum up to give an even number (set-partitioning). In this method  $2^{8m-1}$ - $D_8$ -QAM constellation is generated starting from  $2^{8m}$ - $Z_8$ . The kissing number of  $D_8$  lattice is 112 (calculated through simulation).

### 6.1.3 $E_8$ -QAM

$E_8$ -QAM constellation is based on the  $E_8$  lattice, the most dense lattice structure in eight dimensions known so far [26, 29]. The most convenient method to generate  $E_8$  symbols is through union of  $D_8$  and shifted version of  $D_8$  [26] as described by

$$E_8 = D_8 \cup \left( \left[ \frac{1}{2} \right]_8 + D_8 \right). \quad (6.1)$$

where the  $D_8$  is constructed from the set-partitioning of integer lattice  $Z_8$ .

Alternatively,  $E_8$  consists of points  $x_k = [x_{k,1} \dots x_{k,8}]$  together with the union of points  $y_l = [y_{l,1} \dots y_{l,8}]$ . Such that  $x_k \in Z_8$  and  $\sum_{i=1}^8 x_{k,i}$  is even and  $y_l \in Z_8 + [1/2]_8$  and  $\sum_{i=1}^8 y_{l,i}$  is even. The kissing number of  $E_8$  is 240 [26, Table 1.2].

## 6.2 Selected 8-D Modulations

In this section the performance of few selected 8-D constellations is analysed.

### 6.2.1 128- $D_8$ -QPSK

128- $D_8$ -QPSK has 128 constellation points arranged in  $D_8$  structure which are generated by set partitioning of 256- $Z_8$ -QAM. It is referred to as QPSK since all the constellation points are equal in magnitude. Since 128- $D_8$ -QPSK has only 128 levels, the spectral efficiency is reduced to 7 bits/symbol (1.75 Bit/symbol per channel pair) in comparison to 8 bits/symbol (2 bit/symbol per channel pair) of 256- $Z_8$ -QPSK. But the decrease in SE is very small when compared to the higher asymptotic power efficiency of 2.4304 dB over BPSK.

The maximum number of nearest neighbours in 128- $D_8$ -QPSK is 28. Though the average number of nearest neighbours is high, the SER performance at high SNRs in

comparison with 256- $Z_8$ -QPSK is not degraded due to the higher PE as will be shown in Section 6.3.2.

### 6.2.2 256- $E_8$ -QAM

256- $E_8$ -QAM has 256 constellation points arranged in  $E_8$  structure. It is formed by the union of 128- $D_8$ -QPSK and shifted coset of 128- $D_8$ -QPSK. The centroid of all the points in the union is calculated and moved to origin to minimize  $E_s$ . 256- $E_8$ -QAM has SE of 8 bits/symbol (2 bits/symbol per channel pair) same as the SE of 256- $Z_8$ -QPSK, but has an asymptotic power efficiency of 2.0412 dB compared to 0 dB of 256- $Z_8$ -QPSK.

The maximum number of nearest neighbours of 256- $E_8$ -QAM is 156, but only two symbols have 156 neighbours as shown in Table 6.1.

Table 6.1: Number of neighbours in 256- $E_8$ -QAM constellation.

Type of constellation point ( $k$ )	1	2	3	4	5
No. of nearest neighbours ( $N_k$ )	29	30	36	60	156
No. of constellation points of type $k$ ( $V_k$ )	2	56	140	56	2

## 6.3 Performance of 8-D Modulation Formats

In this section the performance of 8-D modulation formats introduced in the previous sections are discussed.



## 6.3.1 Asymptotic Power Efficiency and Spectral Efficiency

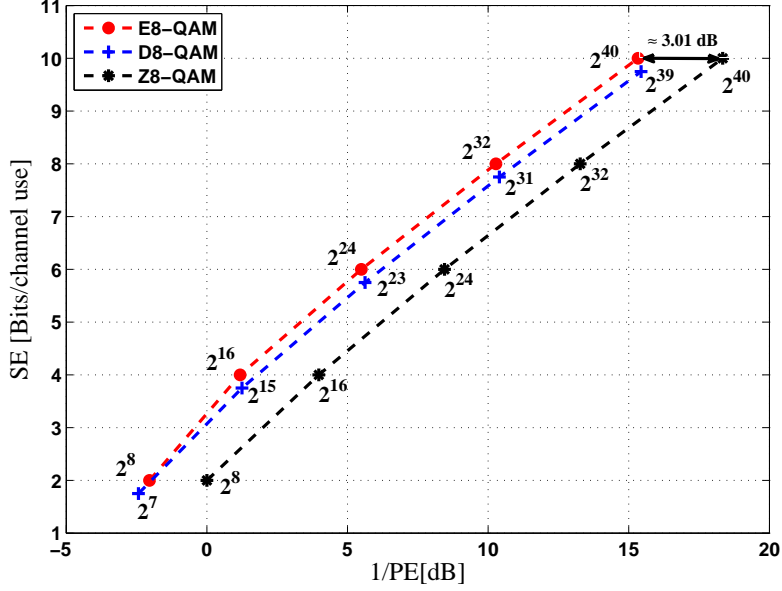

 Figure 6.1: Spectral efficiency vs.  $1/PE$  plot for 8-D modulations.

Figure 6.1 shows spectral efficiency (SE) vs. sensitivity penalty ( $1/PE$ ) plot for  $D_8$ -QAM,  $E_8$ -QAM and  $Z_8$ -QAM modulation formats. Spectral efficiency is normalized to per channel pair for fair comparison. In general the asymptotic gain of  $2^{8m}$ - $E_8$ -QAM is higher than  $2^{8m-1}$ - $D_8$ -QAM except for 256- $E_8$ -QAM. Table 6.2 below compares the asymptotic gain of PS-QPSK, 256- $E_8$ -QAM and  $D_8$ -QPSK over BPSK.

Table 6.2: Asymptotic power efficiencies of selected 8-D modulation formats with PS-QPSK.

	QPSK	PS-QPSK	256- $E_8$ -QAM	$D_8$ -QPSK
Asymptotic gain or PE [dB]	0	1.76	2.041	2.43
SE [Bits/symbol per channel use]	2	1.5	2	1.75

From Table 6.2 it can be concluded that  $D_8$ -QPSK has the highest asymptotic power efficiency with PE=2.43 dB in 8-D, also higher than the 1.76 dB gain of 4-D constellation PS-QPSK.

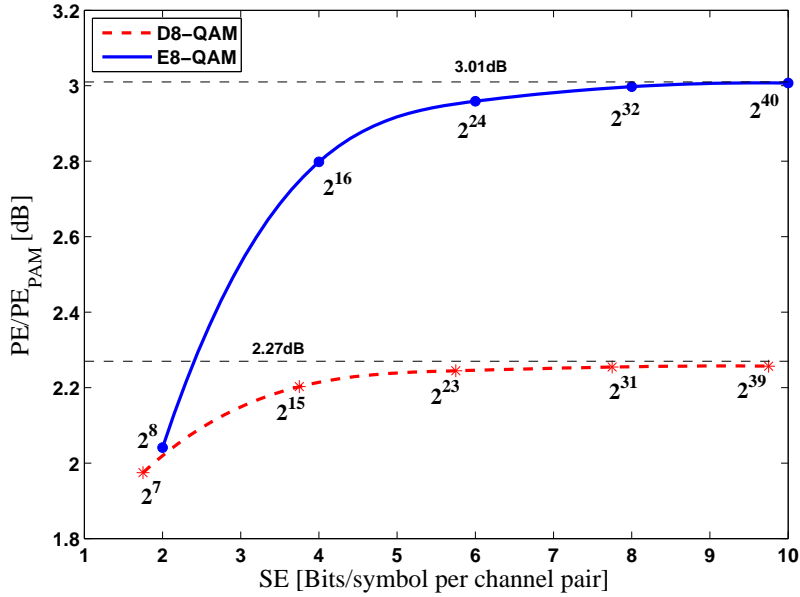


Figure 6.2: PE/PE<sub>PAM</sub> vs. spectral efficiency plot for eight-dimensional modulations. The higher order  $D_8$ -QAM and  $E_8$ -QAM constellations provide coding gains close to the theoretical value of 2.27 dB and 3.01 dB.

Figure 6.2 shows the plot of PE/PE<sub>PAM</sub> with spectral efficiency of  $E_8$ -QAM and  $D_8$ -QAM (similar to the discussion in Section 5.1). The plot shows the maximum gain that can be achieved with respect to base line  $Z_8$ -QAM by using 8-D joint modulation formats. The asymptotic coding gains that can be achieved by using  $E_8$  and  $D_8$  lattices are 3.01 dB and 2.27 dB, respectively [31]. But these maximum gains are achievable if the number of constellation points is high enough to reach the optimal packing density of lattice structures. The packing density as a function of SE of the constellations is shown in Figure 6.3. As seen in the figure, at higher spectral efficiencies the  $E_8$ -QAM and  $D_8$ -QAM constellations attain packing densities close to the theoretical values of  $\frac{\pi^4}{384}$  and  $\frac{\pi^4}{768}$  respectively [26, pp. 121],[34]. Packing density of  $D_8$ -QAM is half the packing density of  $E_8$ -QAM due to the fact that  $E_8$ -QAM is made up of union of  $D_8$ -QAM and its shifted version as described in Eqn. 6.1.  $2^{40}$ - $E_8$ -QAM and  $2^{39}$ - $D_8$ -QAM give gains of 3.007 dB and 2.257 dB, respectively (close to the theoretical limits shown by the dotted lines) as shown in Figure 6.2. The asymptotic gains of  $E_8$ -QAM over  $D_8$ -QAM and SP-QAM are nearly 0.74 dB and 1.5 dB, respectively.

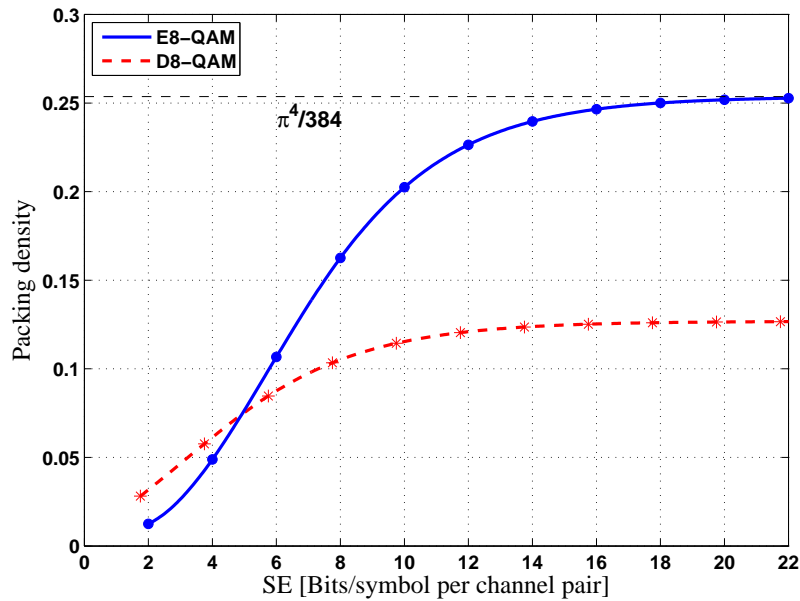


Figure 6.3: Packing density of  $E_8$ -QAM and  $D_8$ -QAM modulation formats with spectral efficiency.

### 6.3.2 Non Asymptotic Performance in AWGN Channel

This section deals with the non asymptotic performance of eight-dimensional modulation in AWGN channel. In  $D_8$ -QAM and  $E_8$ -QAM constellations the number of bits per symbol is less than the kissing number which rules out the possibility of Gray mapping. As a result the BER performance depends on bits to symbol mapping. For this reason SER performance for the constellations is plotted as it does not depend on bits to symbol mapping. Figure 6.4 shows simulated SER curves as a function of SNR for 256- $Z_8$ -QPSK, 128- $D_8$ -QPSK and 256- $E_8$ -QAM. As expected 256- $E_8$ -QAM has better performance when compared to 256- $Z_8$ -QPSK. The performance of 128- $D_8$ -QPSK cannot be compared directly since it has different SE.

The SER curves for the higher order 8-D modulations are not plotted since the simulations are time consuming and the theoretical expressions have not been derived.

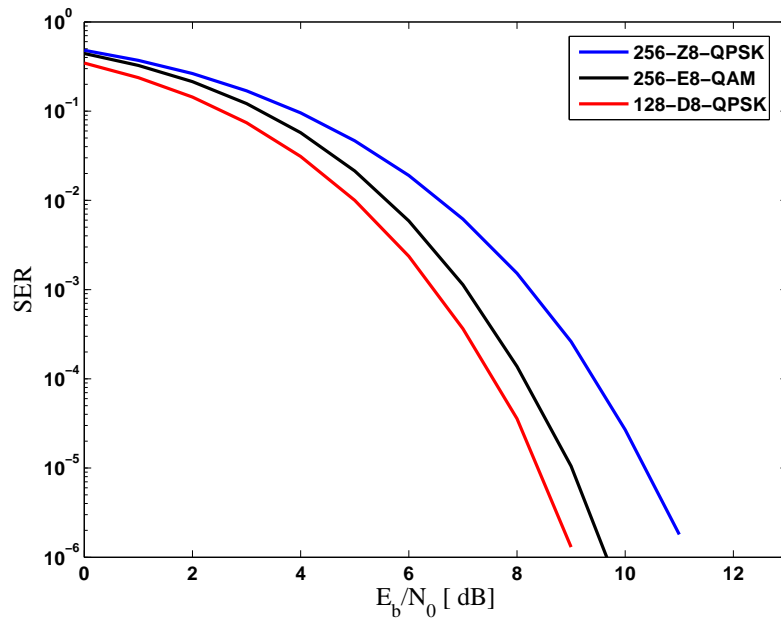


Figure 6.4: SER vs. SNR plots of 8-D modulation formats.

### 6.3.3 Constrained Capacity in AWGN and PC-AWGN Channel

The expression for constrained capacity of a  $N$ -dimensional  $M$ -ary modulation format in AWGN channel is given by Eqn. 5.5. The constrained capacity curves for a few selected 8-D modulation formats are generated using the Monte Carlo simulations and are shown in Figure 6.5.

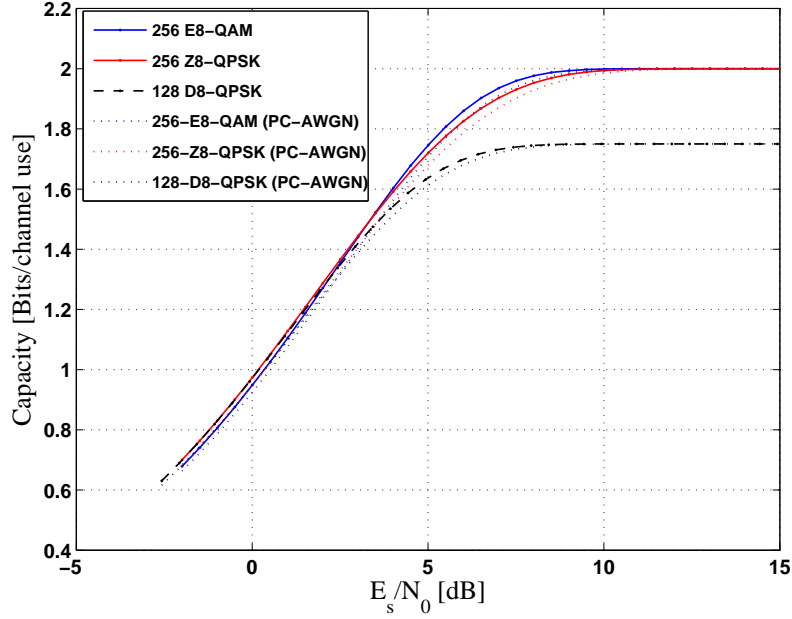


Figure 6.5: Constrained capacity curves for 8-D modulations in AWGN channel.

It can be seen that 256- $E_8$ -QAM requires lower SNR to reach capacity of 1.9 bits in comparison to 256- $Z_8$ -QPSK. Its not fair to compare the capacity curve of 128- $D_8$ -QPSK with 256- $Z_8$ -QPSK since its SE is less than that of 256- $Z_8$ -QPSK and 256- $E_8$ -QAM. An interesting behaviour can be seen in 256- $Z_8$ -QAM and 256- $E_8$ -QAM curves, at low SNRs (nearly up to 3.27 dB) the capacity curve of 256- $Z_8$ -QPSK has higher capacity than 256- $E_8$ -QAM. This is because of the larger kissing number of 256- $E_8$ -QAM. The improvement in capacity curves can be clearly seen at mid SNRs (4 to 10 dB).

The expression for constrained capacity in PC-AWGN channel with Tikhonov distributed phase noise has been derived in Appendix B. Figure 6.5 also shows the capacity curves of 256- $Z_8$ -QPSK, 128- $D_8$ -QPSK and 256- $E_8$ -QAM in PC-AWGN channel with Tikhonov distributed phase noise having  $\rho = 50$ . It can be observed that additional SNR is required to reach a given capacity in PC-AWGN in comparison to AWGN.

## 6.4 Detection of 8-D Modulations

### 6.4.1 Detector for $D_8$ -QAM Constellation Based on Set Partitioning Method

Since the construction of the  $D_8$  from  $Z_8$  is same as the construction of  $D_4$  from  $Z_4$ , the detection algorithm explained in Section 5.4.2 also works for  $D_8$ -QAM. The only difference is that now the symbols are in eight dimensions, in fact this detector is valid for any  $D_N$  lattice regardless of dimensions [29].

### 6.4.2 Detector for $E_8$ -QAM Constellations

By slightly modifying the detector for  $D_8$ -QAM a low complexity detector for  $E_8$ -QAM can be designed. This detection algorithm was suggested in [29].  $E_8$ -QAM constellation is the union of  $D_8$  and its shifted version  $D_8 + [\frac{1}{2}]_8$ . The received symbol will lie either on  $D_8$  lattice or its shifted version  $D_8 + [\frac{1}{2}]_8$ . By detecting the received symbol separately with  $D_8$  and its shifted version  $D_8 + [\frac{1}{2}]_8$  and then deciding among two possible candidates a low complexity detector for  $E_8$ -QAM can be designed. The discussed detector performs maximum likelihood detection. The block diagram of the detector algorithm is shown in Figure 6.6.

To understand the working of the detector, consider one of the methods used to generate  $E_8$  constellations. The block on the left side in Figure 6.6 shows how  $E_8$  constellation is generated starting from the cubic lattice  $Z_8$  and its shifted version  $R_8$ .  $E_8$  symbols are formed by union of two  $D_8$ , one that is generated by set partitioning of  $Z_8$  i.e.,  $D_8$  A which is made up of points  $x_k \in Z_8$  such that  $\sum_{i=1}^8 x_{k,i}$  is even and the other that is generated by the set partitioning of  $R_8 = Z_8 + [1/2]_8$  i.e.,  $D_8$  B which is made up of points  $y_l \in R_8$  such that  $\sum_{i=1}^8 y_{l,i}$  is even.

Consider the sampled received symbol  $r = c + w$ , where  $c$  is the 8-D symbol chosen from  $E_8$ -QAM. The constellation points in  $Z_8$  and  $R_8$  closest to and next closest to  $r$  are determined to result in  $c'_1, c''_1, c'_2$  and  $c''_2$  as shown in Figure 6.6. Among the four outputs the ones belonging to  $D_8$  A and  $D_8$  B are picked resulting in  $c_1$  and  $c_2$ . Now the received symbol  $r$  has two possible constellation points as transmitted symbol. Among  $c_1$  and  $c_2$  the one closer to  $r$  is determined and referred as  $c'$  which is the detected constellation point.

## Summary

In this chapter, joint modulation formats in eight dimensions were discussed. Asymptotic power efficiencies and spectral efficiencies of the  $D_8$  and  $E_8$  constellations were compared to the  $Z_8$  constellations. The asymptotic power gains of 2.041 dB for 256- $E_8$ -QAM and 2.43 dB for 128- $D_8$ -QPSK were shown over 256- $Z_8$ -QAM. Simulated SER curves and constrained capacity curves for a few selected modulation were plotted. Finally a low complexity algorithm for detection of  $E_8$  constellations was discussed.

From the results of Chapter 5 and this chapter, the performance of joint modulation formats in higher dimensions can be generalized. As the dimension of the modulation formats is increased the asymptotic power efficiency of joint modulation increases for a fixed SE. It has been shown that asymptotic gains upto 1.51 and 3.01 dB can be achieved in four and eight dimensions, respectively. These gains obtained are asymptotic in nature and give faint idea regarding the SER performance of the constellation in presence of noise.

In presence of noise the average number of neighbours a constellation point has, affects the SER performance of the modulation format. When comparing SER perfor-

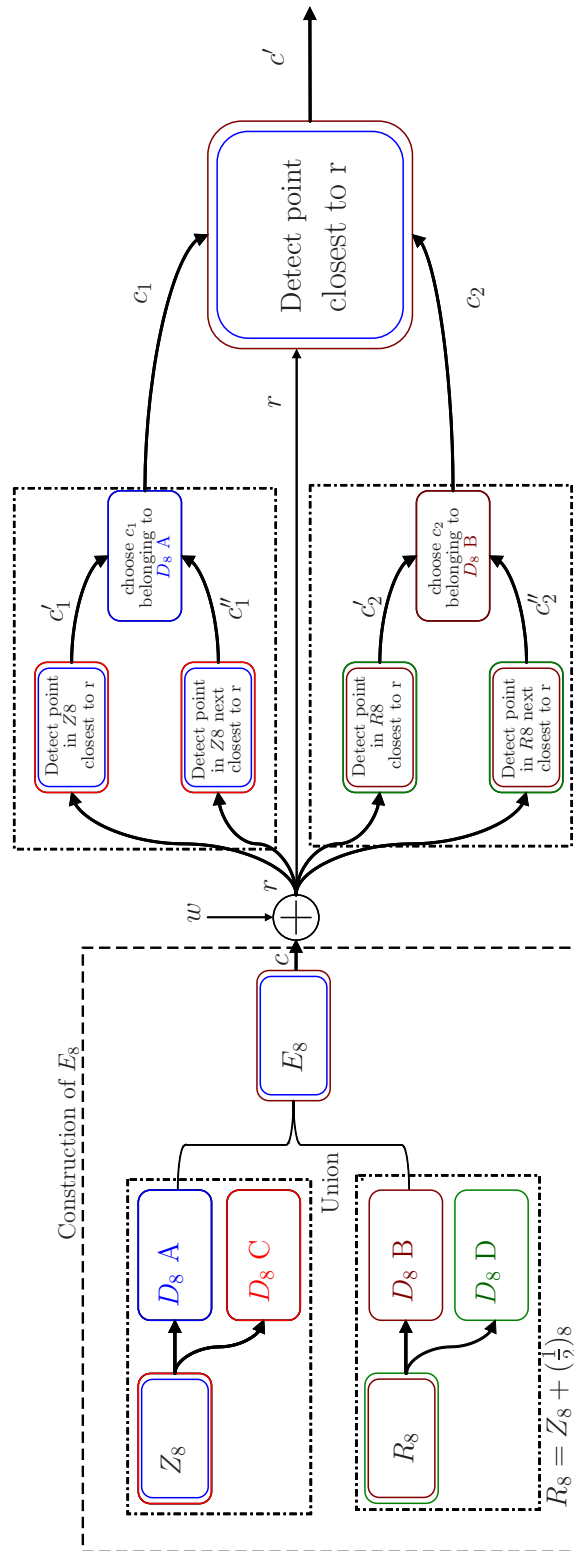


Figure 6.6: Block diagram showing the construction and detection of  $E_8$ -QAM constellation.

mance of two constellations having same SE, the constellations having higher asymptotic gains but also higher average number of neighbours may start performing better than the other constellation after a specific SNR. Figure 6.7 shows the SER curves of two arbitrary constellations referred to as MOD-A and MOD-B. The constellation MOD-B has higher asymptotic gain than MOD-A but also higher average number of neighbours, as a result MOD-B starts performing better after a SNR shown in the figure. This SNR after which the constellation starts performing better is a function of asymptotic gain and average number of neighbours. This SNR and the corresponding SER can be called as cross over SNR and cross over SER.

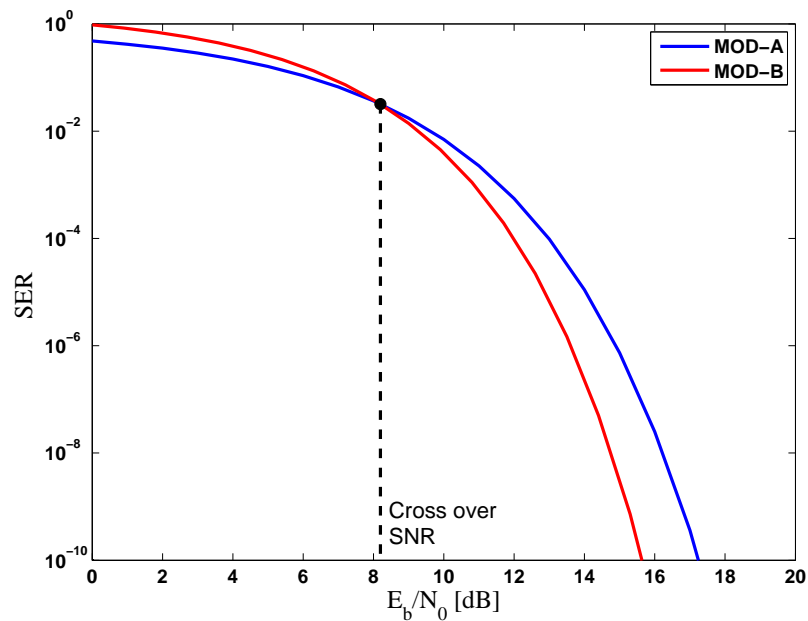


Figure 6.7: Cross over SNR of two arbitrary modulation formats MOD-A and MOD-B having same SE.

This cross over SNR could be as low as zero dB for a lower order  $N$ -dimensional constellation and could also be significantly high for a higher order  $N$ -dimensional constellation in comparison with cubic constellation of same SE. For 256- $E_8$ -QAM constellation the cross over SNR is nearly 0 dB, which makes it practically feasible even at lower SNRs.



## Chapter 7

# Conclusion and Future work

The following results and conclusions have been drawn from the thesis work.

- The joint processing of independent communication streams obtained from polarization multiplexing or spatial separation gives rise to higher dimensional signal space with higher DOF. The higher DOF can be used to obtain power efficient or spectrally efficient modulation formats.
- The most dense packing structure in four dimensions, the  $D_4$  lattice structure can be used to construct power efficient modulation formats. The modulation formats are referred to as Spherical- $D_4$  and SP-QAM. The higher order SP-QAM constellations give an asymptotic gain of 1.51 dB over the DP-QAM constellations.
- The increased power efficiency of the joint modulation formats was interpreted in terms of spectral efficiency and the SP-QAM modulation formats were also shown to be spectrally efficient.
- The SP-QAM constellations were shown to provide an additional SE of 0.5 Bit/Symbol per polarization over the DP-QAM constellations while keeping the performance unaltered at  $\text{SER}=10^{-7}$ .
- The performance of the SP-QAM constellations in AWGN channel was analysed and theoretical expression for the nearest neighbour approximation SER of SP-QAM constellations was derived. Further, capacity curves for a few selected 4-D joint modulation formats were plotted for AWGN channel and PC-AWGN channel with Tikhonov-distributed phase noise.

- 
- Two low complexity detectors for SP-QAM constellations were discussed which perform Maximum Likelihood detection.
  - The possibility of eight DOF in  $4 \times 4$  SS-DP LoS MIMO links and dense structures in 8-D were discussed. 8-D modulation formats based on the  $D_8$  and  $E_8$  lattice structures were constructed.
  - The  $D_8$ -QAM and  $E_8$ -QAM constellations constructed were shown to provide an asymptotic gain of 2.27 dB and 3.01 dB respectively for higher order constellations. The selected modulation formats 128- $D_8$ -QPSK and 256- $E_8$ -QAM give asymptotic gains of 2.43 and 2.041 dB, respectively.
  - The performance of selected 8-D modulation formats was analysed and capacity curves were plotted. Low complexity detectors for  $D_8$  and  $E_8$  constellation were also discussed.
  - It is shown that significant gains in power and spectral efficiency can be obtained by using joint modulations in four and eight dimensions. Further, low complexity detectors also exist which make the joint modulations feasible for practical applications.

## Future work

1. **Synchronization:** A brief account on the misalignment of symbols from independent streams causing error in detection was mentioned in Section 5.5 and a technique to overcome the problem was also discussed. More robust techniques having less overhead have to be developed.
2. **Gain control:** The gains in the horizontal and vertical polarization channels play an important role in the detection of the symbols. From the discussion in the previous chapters the symbol in four dimensions can be considered equivalent to 4-D sphere. If the gains in the horizontal and vertical polarizations are different, the symbols can no longer be regarded as spheres and they are equivalent to ellipsoids. Detection of such symbols results in higher number of errors. To prevent this, the signals from both polarizations have to be scaled individually to result in a symbol that is equivalent to a sphere. This scaling has to be done both at the receiver and transmitter through feed-back so as to keep the signal to noise ratio same on both polarizations.

- 
3. **Phase noise:** Phase noise is a critical factor in high frequency microwave systems operating in K bands and above due to high oscillator phase noise. Analog and DSP techniques are used to counter the effect of phase noise in systems treating the two polarizations separately. The effect of phase noise on the joint modulation formats discussed in the thesis has to be studied and techniques to overcome the effect have to be worked on.
  
  4. The joint modulation formats and their performance has been discussed in the thesis by ignoring some aspects of communication system such as equalizer, non-linearities and I-Q imbalance. The effect of these on the performance of the joint modulations gives a wide scope for future work.
  
  5. The proposed 4 and 8-D constellations can be used in the design of coded-modulation schemes to improve their power efficiency [35].

## Appendix A

# Union Bound for Theoretical Symbol Error Rate

The union bound of the SER is obtained by considering the pair-wise error probability ( $P_{\text{pep}}$ ) and nearest neighbours approximation. The expression derived in this appendix is used in the section 5.2 to plot the nearest neighbour approximation SER curves. When calculating the  $P_{\text{pep}}$ , a pair of adjacent constellation points are considered and the presence of other constellation points is ignored. Let the two adjacent constellation points be  $c_1$  and  $c_2$ . The  $P_{\text{pep}}$  is defined as the probability that  $c_1$  is transmitted and  $c_2$  is detected or vice-versa,

$$P_{\text{pep}} = p(c_1|c_2) = p(c_2|c_1).$$

In an  $N$ -dimensional constellation the  $(N - 1)$ -dimensional plane bisecting the line joining the two constellation points perpendicularly decides the decision regions of the point.

Consider two adjacent constellation points in SP-QAM A constellation. The constellation points in SP-QAM A are such that they differ only in two co-ordinates, for example  $c_1=[a,a,b,c]$  and  $c_2=[a,a,d,e]$ . The distance between the points is  $d_{\text{min}}$  and from the geometry of SP-QAM A  $|b - d| = |c - e| = \frac{d_{\text{min}}}{\sqrt{2}}$ .

Consider the transmission of  $c_1$  over the AWGN channel. The probability distribution of the received symbol  $r = c_1 + w$  is a four-dimensional Gaussian having mean at  $c_1=[a,a,b,c]$ . The probability that the received symbol  $r$  is detected as  $c_2$  is the volume of the pdf lying in the decision region of  $c_2$ . Since the points considered share co-ordinates in two dimensions the noise components in those two dimensions do not affect the detection of symbol. As a result the  $P_{\text{pep},d_{\text{min}}}$  can be obtained by only integrating the pdf of the noise components affecting the symbol detection.

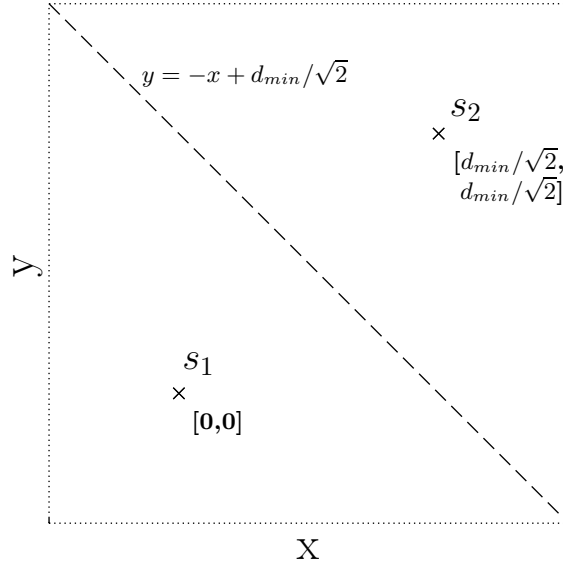


Figure A.1: Two adjacent constellation points considered for calculating  $P_{\text{pep}}$ .

The problem now reduces to calculating the  $P_{\text{pep}}$  between the points  $s_1=[b,c]$  and  $s_2=[d,e]$ . Since  $|b-d| = |c-e| = \frac{d_{\text{min}}}{\sqrt{2}}$ , the points can be replaced with  $s_1=[0,0]$  and  $s_2=[\frac{d_{\text{min}}}{\sqrt{2}}, \frac{d_{\text{min}}}{\sqrt{2}}]$ . The figure A.1 shows the constellation points  $s_1$  and  $s_2$  and their decision regions determined by the dashed line. Considering the transmission of  $s_2$  over an AWGN channel, the  $P_{\text{pep}}$  can be expressed as [22, Eqn. 4.29]

$$P_{\text{pep},d_{\text{min}}} = \frac{1}{2} \text{erfc} \left( \frac{d_{\text{min}}}{2\sqrt{N_0}} \right).$$

## Appendix B

# Constrained Capacity Curves in PC-AWGN channel

PC-AWGN channel model is a combination of both AWGN and phase noise. In this section Tikhonov distribution for phase noise is considered for deriving the constrained capacity expressions since it closely models the residual phase error when a phase-locked loop is used at the receiver [15, 16].

The expression for the conditional output distribution of the PC-AWGN channel when the Tikhonov phase noise model considered has been derived in [33] as

$$P_{Y|X}(y|x) = \int_{-\pi}^{\pi} p_W(y - xe^{i\theta})p_{\Theta}(\theta)d\theta, \quad (\text{B.1})$$

where  $p_W$  is the probability distribution function of AWGN  $W$  and  $p_{\Theta}(\theta)$  is the probability distribution function of Tikhonov distributed phase noise, i.e.,

$$W \sim \mathcal{N}(0, 2\sigma^2),$$

$$p_{\Theta}(\theta) = \begin{cases} \frac{e^{\rho \cos(\theta)}}{2\pi I_0(\rho)}, & \text{if } \theta \in [-\pi, \pi] \\ 0, & \text{if } \theta \notin [-\pi, \pi] \end{cases},$$

where  $\rho$  is a parameter of the Tikhonov distribution and is related to the variance of the angle  $\theta$  as  $\rho \propto \frac{1}{\sigma_{\theta}^2}$ .  $I_0(\rho)$  is the zero order Bessel function of first kind. Substituting these in the expression for  $P_{Y|X}(y|x)$  we have

$$P_{Y|X}(y|x) = \frac{1}{(2\pi\sigma)^2 I_0(\rho)} \int_{-\pi}^{\pi} e^{\rho \cos(\theta) - \frac{|y - xe^{i\theta}|^2}{2\sigma^2}} d\theta.$$

The expression has to be extended for higher dimensional modulations. In higher dimensional modulations a pair of  $I$  and  $Q$  components of the same carrier are modulated by a single oscillator and demodulated at the receiver by another oscillator. The phase noises at the transmitter and receiver can be regarded as a single random process having

a variance equal to sum of individual variances. As a consequence a pair of dimensions experience a different phase noise process. To derive the constrained capacity curves for higher dimensional modulations the phase noise process on each pair are assumed to be independent and identical, this changes the channel model to

$$y = x' + w,$$

where  $x'$  is the transmitted symbol affected by the phase noise. Splitting  $y$ ,  $x'$  and  $w$  into two 2-D vectors corresponding to separate polarizations, the channel model can be expressed as

$$[y_h, y_v] = [x_h e^{i\theta_h}, x_v e^{i\theta_v}] + [w_h, w_v], \quad (\text{B.3})$$

where subscript  $h$  and  $v$  correspond to the horizontal and vertical polarization.

For a dual polarized system with the assumptions stated above, the horizontal and vertical polarization components experience independent and identical phase noise processes. The phase noise distribution can be written as,

$$p_{\Theta_h, \Theta_v}(\theta_h, \theta_v) = p_{\Theta_h}(\theta_h) \cdot p_{\Theta_v}(\theta_v). \quad (\text{B.4})$$

As a result the expression for the conditional output distribution of the PC-AWGN channel becomes

$$\begin{aligned} P_{Y|X}(y|x) &= \int_{-\pi}^{\pi} \int_{-\pi}^{\pi} p_W(y - x') p_{\Theta_h}(\theta_h) \cdot p_{\Theta_v}(\theta_v) d\theta_h d\theta_v \\ &= \int_{-\pi}^{\pi} p_W(y_h - x_h e^{i\theta_h}) p_{\Theta_h} d\theta_h \cdot \int_{-\pi}^{\pi} p_W(y_v - x_v e^{i\theta_v}) p_{\Theta_v} d\theta_v. \end{aligned} \quad (\text{B.5})$$

The above equation is obtained by assuming Gaussian noise is independent of phase noise. Following the procedure in [33, pp. 32-33] we get the expression for constrained capacity in PC-AWGN Channel with Tikhonov distributed phase noise as

$$\begin{aligned} I(X; Y) &= \log_2(M) - \frac{1}{M} \sum_{x \in \mathcal{X}} \mathbb{E}_{Y|X} \left[ \log_2 \left( \sum_{x' \in \mathcal{X}} \exp \left( \frac{|x|^2 - |x'|^2}{2\sigma^2} \right) \right. \right. \\ &\times \left. \left. \frac{I_0(\sigma^{-2} \sqrt{(\Re\{y_h^* x'_h\} + \rho\sigma^2)^2 + (\Im\{y_h^* x'_h\})^2})}{I_0(\sigma^{-2} \sqrt{(\Re\{y_h^* x_h\} + \rho\sigma^2)^2 + (\Im\{y_h^* x_h\})^2})} \cdot \frac{I_0(\sigma^{-2} \sqrt{(\Re\{y_v^* x'_v\} + \rho\sigma^2)^2 + (\Im\{y_v^* x'_v\})^2})}{I_0(\sigma^{-2} \sqrt{(\Re\{y_v^* x_v\} + \rho\sigma^2)^2 + (\Im\{y_v^* x_v\})^2})} \right) \right] \end{aligned}$$

The expression can be further extended to higher dimensional constellations by treating the phase noise processes on a pair of dimensions as independent and identical. The expression derived in this appendix has been used in Section 5.3.2 and 6.3.3 for plotting the constrained capacity curves in PC-AWGN channel.

# Bibliography

- [1] M. Karlsson and E. Agrell, “Which is the most power-efficient modulation format in optical links?” *Optics Express*, vol. 17, no. 13, pp. 10 814 – 10 819, Jun. 2009.
- [2] F. Bøhagen, P. Orten, and G. E. Øien, “Optimal design of uniform planar antenna arrays for strong line-of-sight MIMO channels,” in *IEEE 7th Workshop on Signal Processing Advances in Wireless Communications*, Jul. 2006, pp. 1 – 5.
- [3] T. Ingason, H. Liu, M. Coldrey, A. Wolfgang, and J. Hansryd, “Impact of frequency selective channels on a line-of-sight MIMO microwave radio link,” in *IEEE 71st Vehicular Technology Conference (VTC 2010-Spring)*, May 2010, pp. 1 – 5.
- [4] P. Noel, M. Prokoptsov, M. Klemes, H. Tai, A. Dufour, and K. Morris, “The design, development and implementation of a cross-polarization interference cancellation system for point-to-point digital microwave radio systems,” in *24th Canadian Conference on Electrical and Computer Engineering (CCECE)*, May 2011, pp. 001 365 – 001 369.
- [5] M. T. Core, “Cross polarization interference cancellation for fiber optic systems,” *Journal of Lightwave Technology*, vol. 24, no. 1, pp. 305 – 312, Jan. 2006.
- [6] M. Borgne, “A new class of adaptive cross-polarization interference cancellers for digital radio systems,” *IEEE Journal on Selected Areas in Communications*, vol. 5, no. 3, pp. 484 – 492, Apr. 1987.
- [7] G. Welti and J. Lee, “Digital transmission with coherent four-dimensional modulation,” *IEEE Transactions on Information Theory*, vol. 20, no. 4, pp. 497 – 502, Jul. 1974.
- [8] G. Taricco, E. Biglieri, and V. Castellani, “Applicability of four-dimensional modulations to digital satellites: a simulation study,” in *IEEE Global Telecommunications Conference*, vol. 4, Nov. 1993, pp. 28 – 34.
- [9] S. Betti, F. Curti, G. De Marchis, and E. Iannone, “A novel multilevel coherent optical system: 4-quadrature signaling,” *Journal of Lightwave Technology*, vol. 9, no. 4, pp. 514 – 523, Apr. 1991.



- [10] E. Agrell and M. Karlsson, "Power-efficient modulation formats in coherent transmission systems," *Journal of Lightwave Technology*, vol. 27, no. 22, pp. 5115 – 5126, Nov. 2009.
- [11] M. Sjödin, P. Johannisson, H. Wymeersch, P. A. Andrekson, and M. Karlsson, "Comparison of polarization-switched QPSK and polarization-multiplexed QPSK at 30 gbit/s," *Optics Express*, vol. 19, no. 8, pp. 7839 – 7846, Apr. 2011.
- [12] L. Coelho and N. Hanik, "Global optimization of fiber-optic communication systems using four-dimensional modulation formats," in *37th European Conference and Exposition on Optical Communications*. Optical Society of America, 2011, p. Mo.2.B.4.
- [13] U. Madhow, "*Fundamentals of Digital Communication*". Cambridge University Press, 2008.
- [14] T. Ingason and H. Liu, "Line-of-sight MIMO for microwave links," Master's thesis, Department of Signals and Systems, Chalmers University of Technology, Sweden, no. EX064/2009, 2009.
- [15] A. J. Viterbi, "Phase-locked loop dynamics in the presence of noise by Fokker-Planck techniques," *Proceedings of the IEEE*, vol. 51, no. 12, pp. 1737 – 1753, Dec. 1963.
- [16] C. M. Lo and W. H. Lam, "Error probability of binary phase shift keying in Nakagami-m fading channel with phase noise," *Electronics Letters*, vol. 36, no. 21, pp. 1773 – 1774, Oct. 2000.
- [17] A. Goldsmith, "*Wireless Communications*". Cambridge University Press, 2005.
- [18] A. J. Paulraj, D. A. Gore, R. U. Nabar, and H. Bölcskei, "An overview of MIMO communications - a key to gigabit wireless," *Proceedings of the IEEE*, vol. 92, no. 2, pp. 198 – 218, Feb. 2004.
- [19] J. Hansryd and J. Edstam, "Microwave capacity evolution," *Ericsson review*, 2011, <http://www.ericsson.com/res/docs/review/Microwave-Capacity-Evolution.pdf>.
- [20] M. Coldrey, "Modeling and capacity of polarized MIMO channels," in *IEEE Vehicular Technology Conference, 2008*, May 2008, pp. 440 – 444.
- [21] M. K. Simon and M. Alouini, "A unified approach to the performance analysis of digital communication over generalized fading channels," *Proceedings of the IEEE*, vol. 86, no. 9, pp. 1860 – 1877, Sep. 1998.
- [22] S. Benedetto and E. Biglieri, *Principles of Digital Transmission: With Wireless Applications*. Norwell, MA, USA: Kluwer Academic Publishers, 1999.
- [23] M. Karlsson and E. Agrell, "Power efficient modulation schemes," in *Impact of Nonlinearities on Fiber Optic Communications*, S. Kumar, Ed. Springer, 2011, pp. 219 – 252.

## BIBLIOGRAPHY

---

- [24] G. D. Forney, Jr. and L.-F. Wei, “Multidimensional constellations. I. introduction, figures of merit, and generalized cross constellations,” *IEEE Journal on Selected Areas in Communications*, vol. 7, no. 6, pp. 877 – 892, Aug. 1989.
- [25] W. Mao and J. M. Kahn, “Lattice codes for amplified direct-detection optical systems,” *IEEE Transactions on Communications*, vol. 56, no. 7, pp. 1137 – 1145, Jul. 2008.
- [26] J. H. Conway and N. J. A. Sloane, *Sphere Packings, Lattices and Groups*, 3rd ed. Springer-Verlag, NY, 1999.
- [27] S.-J. Park, “Triangular quadrature amplitude modulation,” *Communications Letters, IEEE*, vol. 11, no. 4, pp. 292 – 294, Apr. 2007.
- [28] J. H. Conway and N. J. A. Sloane, “What are all the best sphere packings in low dimensions?” *Discrete Computational Geometry*, vol. 13, pp. 383 – 403, 1995, 10.1007/BF02574051. [Online]. Available: <http://dx.doi.org/10.1007/BF02574051>
- [29] J. H. Conway and N. J. A. Sloane, “Fast quantizing and decoding and algorithms for lattice quantizers and codes,” *IEEE Transactions on Information Theory*, vol. 28, no. 2, pp. 227 – 232, Mar. 1982.
- [30] M. Karlsson and E. Agrell, “Spectrally efficient four-dimensional modulation,” in *Optical Fiber Communication Conference*. Optical Society of America, Mar. 2012, p. OTu2C.1.
- [31] G. D. Forney, Jr., “Coset codes. I. introduction and geometrical classification,” *IEEE Transactions on Information Theory*, vol. 34, no. 5, pp. 1123 – 1151, Sep. 1988.
- [32] C. E. Shannon, “A mathematical theory of communication,” *The Bell Systems Technical Journal*, vol. 27, pp. 379 – 423, 623 – 656, 1948.
- [33] Y. Lejosne, “Results on the constrained capacity for phase noise channels,” Master’s thesis, Department of Signals and Systems, Chalmers University of Technology and Telecom Bretagne, 2011.
- [34] E. W. Weisstein. Hypersphere packing, From MathWorld—A Wolfram Web Resource. [Online]. Available: <http://mathworld.wolfram.com/HyperspherePacking.html>
- [35] L. Beygi, E. Agrell, and M. Karlsson, “On the dimensionality of multilevel coded modulation in the high SNR regime,” *IEEE Communications Letters*, vol. 14, no. 11, pp. 1056 – 1058, Nov. 2010.